

Quantum theory of the dc Josephson effect: Static tunneling characteristics of ultrasmall Josephson junctions

D. Rogovin

Rockwell International Science Center, 1049 Camino dos Rios, Thousand Oaks, California 91360

J. Nagel

Bell Laboratories, Crawford Road, Holmdell, New Jersey 07733

(Received 28 December 1981; revised manuscript received 13 May 1982)

We examine the static tunneling characteristics of ultrasmall Josephson junctions that are current biased on the zero-voltage dc step. Novel scaling, magnetic, and thermal characteristics are exhibited by the supercurrent as the device is scaled down from the 1.0 to the 0.01 μm^2 regime. Furthermore, the noise voltage is found to peak for devices in which the electrostatic energy required to transfer a pair is equal to the interaction energy between the two superconductors. For such junctions, noise voltages are on the order of several mV, and the magnitude of the supercurrent is found to be a very sensitive function of device area and operating temperature. Finally, these features of the junction's dynamics have technological implications regarding digital applications of such devices.

I. INTRODUCTION

Recently, there has been considerable interest in the physics and technology of ultrasmall Josephson junctions.¹ This interest is motivated by the digital applications of these devices² as well as the possibility of novel physical behavior arising from the large electrostatic energies associated with ultralow capacitance junctions.³ Here we examine the static tunneling characteristics of ultrasmall Josephson junctions that are current biased on the zero-voltage dc step. We are particularly concerned with changes in the junction's tunneling characteristics that may occur as the device is scaled down from dimensions on the order of 1 μm^2 to less than 0.01 μm^2 . Of special interest are the influence of electrostatic fluctuations on the magnitude, scaling characteristics, and phase dependence of the dc supercurrent. Furthermore, the response of these junctions to magnetic fields as well as their thermal characteristics are clearly important with regard to their usefulness as switching elements in digital devices. Owing to the small size of the supercurrent, interest naturally focuses on the current and voltage fluctuations that accompany pair transfer as well as the signal-to-noise ratio of the pair current. These features of the junction's dynamics are examined in detail, although no account is taken of the effects of fluctuation induced switching on the pair current, which we shall discuss elsewhere. We note that

these studies not only provide a knowledge of the physics of ultrasmall Josephson junctions but are of critical importance for determining the limiting size, packing density, and switching speeds for digital applications of these devices. For example, we find that the supercurrent exhibits a striking dependence on device size and temperature as the junction area is scaled down from 1.0 to 0.01 μm^2 . These properties in turn impact device fabrication, thermal tolerances, and switching reliability, the degree depending upon a number of factors, which are discussed in this paper.

To illustrate the influence of electrostatic effects on pair transfer we examine and contrast the junction's tunneling characteristics in three different regimes. These are (1) the tight-binding limit in which there are no electrostatic effects, (2) the plasmon regime in which electrostatic effects give rise to plasma oscillations, and (3) the strong charge-fluctuation regime where electrostatic effects quench the phase ordered state between the two superconducting electrodes. In these regimes analytic expressions can be obtained for various physical quantities of interest. Numerical results are also presented to examine changes in the junction's behavior as it passes from one regime to another.

In Sec. II we present a quantum formulation of the dc Josephson effect that enables us to examine the effect of electrostatic fluctuations on pair transfer for arbitrarily small values of the junction

capacitance.⁴ We also discuss an interesting analogy between a Josephson junction and a two-dimensional rotating dipole in a dc electric field. This analogy is useful for understanding many of the novel features of ultrasmall Josephson junctions.

In Sec. III we examine the tunneling characteristics of the normalized current amplitudes A_l defined by

$$A_l(\phi) \equiv I_l(\phi)/(J \sin \phi), \quad (1.1)$$

where the pair-current matrix elements I_l are defined by

$$I_l(\phi) \equiv \langle \psi_l(\phi) | \hat{I} | \psi_l(\phi) \rangle. \quad (1.2)$$

Here $|\psi_l(\phi)\rangle$ is the eigenvector for the l th state and \hat{I} is the current operator. We discuss the magnitude, phase dependence, and scaling and thermal characteristics of the various normalized current amplitudes in ultrasmall Josephson junctions. We also consider the response of these amplitudes to a static magnetic field. In general, we find that different junction states exhibit different tunneling characteristics. These differences arise from and reflect the fact that electrostatic fluctuations distort the phase order of the different $|\psi_l(\phi)\rangle$ in varying ways.

In Sec. IV we discuss the tunneling characteristics of the dc pair current in ultrasmall Josephson junctions. We examine the phase dependence, magnitude as well as the scaling, magnetic, and thermal characteristics of the supercurrent. Because the different junction states have markedly different pair-transfer characteristics, novel physical behavior is displayed by the supercurrent once these states are thermally activated.

In Sec. V we examine the current and voltage fluctuations of ultrasmall Josephson junctions that are current biased on the zero-voltage dc step. Of particular interest is the fact that the rms noise voltage peaks when the electrostatic energy required to transfer a pair is on the order of the interaction energy of the two superconducting electrodes. For smaller values of the capacitance, the rms noise voltage is found to decrease, eventually reaching a value which is independent of the junction's capacitance and set by the interaction energy between the two superconductors. We also discuss the current and voltage fluctuation spectra as well as the signal-to-noise ratio of the pair current for ultrasmall Josephson junctions.

Finally, in Sec. VI we summarize our results and discuss some of the technological implications of this research regarding digital applications of ultrasmall Josephson junctions.

II. QUANTUM FORMULATION OF THE dc JOSEPHSON EFFECT

In this section we review our quantum formulation of the dc Josephson effect for a junction that is current biased on the zero-voltage dc step. In Sec. IIA we introduce a number of parameters that are useful for discussing the tunneling characteristics of ultrasmall Josephson junctions. In Sec. IIB we review the operator algebra and the tunneling eigenvalue problem for a Josephson junction that is current biased on the zero-voltage dc step. In Sec. IIC we discuss the relationship of this work, which is formulated in the definite-number representation, to more standard treatments that are formulated in the definite-phase representation. In Sec. IID we present a model of the external drive circuit using a density-matrix approach and discuss its nature in both the definite-number and definite-phase representations. We show that Anderson's model⁵ of the external circuit can be extracted from ours for large junctions that are not driven too far from equilibrium. For small junctions this is not the case, and we discuss this point in some detail. In Sec. IIE we present an interesting analogy between a Josephson junction and a two-dimensional rotating dipole in a dc electric field.

A. Electrostatic parameters

Section II is concerned with a quantum formulation of the dc Josephson effect, which enables one to determine the influence of electrostatic fluctuations on the static pair-transfer characteristics for arbitrarily small devices. We are particularly concerned with the regime in which

$$2e^2/C \gtrsim E, \quad (2.1)$$

where $E = \hbar J/2e$ with J the critical current amplitude. It is natural then to characterize the role of electrostatic fluctuations by the quantity

$$\sigma \equiv \frac{E}{2e^2/C} \quad (2.2)$$

and note that as $\sigma \rightarrow 0$ the Josephson effect is quenched by electrostatic fluctuations. The value $\sigma = 1$, defines a critical surface area S_C expressed in μm^2 ,

$$S_C \equiv 1.327 \left[\frac{t}{j\epsilon} \right]^{1/2} \times 10^{-2}, \quad (2.3)$$

where t , the oxide width, is in units of 10^{-9} m, ϵ is

the ratio of the oxide's dielectric constant to that of vacuum, and j is the critical current density in units of 10^8 A/m². Typically, $l \sim 5$, $j \sim 1$, $\epsilon \sim 5$ so that $S_C \sim 0.01$ μm^2 , and for a device of this size, $J \sim 1$ μA , $C \sim 10^{-4}$ pF, which defines the junction parameters of interest to us.

B. Zero-voltage current-biased eigenstates and eigenvalues

For our purposes, it is most convenient to work in the definite-number representation that uses as basis vectors the pair difference states $|n\rangle$ defined by⁶

$$|n\rangle \equiv |N+n\rangle_L \otimes |N-n\rangle_R, \quad (2.4)$$

where $|N+n\rangle$ is the state vector for a superconductor with n excess pairs in the definite number representation. The junction Hamiltonian consists of an electrostatic term plus a tunneling term,

$$\hat{H} = \frac{(2e\hat{n})^2}{2C} - (\hat{H}_T^+ + \hat{H}_T^-), \quad (2.5)$$

where \hat{n} is the pair number difference operator and \hat{H}_T^+ (\hat{H}_T^-) transfers a pair from left (right) to right (left). The quantum structure of these operators is set by their matrix elements

$$\langle n | \hat{n} | n' \rangle = n \delta_{n,n'}, \quad (2.6a)$$

$$\langle n | \hat{H}_T^\pm | n' \rangle = \frac{1}{2} E(n) \delta_{n,n' \pm 1}. \quad (2.6b)$$

A convenient representation of Eqs. (2.6) is

$$\hat{n} = \sum_n n |n\rangle \langle n|, \quad (2.7a)$$

$$\hat{H}_T^\pm = \frac{1}{2} \sum_n E(n) |n\rangle \langle n \mp 1|. \quad (2.7b)$$

Equations (2.7) imply the following commutation relations:

$$[\hat{n}, \hat{H}_T^\pm] = \pm \hat{H}_T^\pm \quad (2.8a)$$

$$[\hat{H}_T^+, \hat{H}_T^-] = \frac{1}{4} \sum_n E(n) [E(n+1) - E(n-1)] \times |n\rangle \langle n|. \quad (2.8b)$$

If we neglect the voltage dependence of J , then E is independent of n and the commutation relations reduce to

$$[\hat{n}, \hat{H}_T^\pm] = \pm \hat{H}_T^\pm, \quad (2.9a)$$

$$[\hat{H}_T^+, \hat{H}_T^-] = 0. \quad (2.9b)$$

To obtain the junction eigenstates and eigenvalues

we expand the state vector in terms of definite-number states, in particular for the l th state

$$|\psi_l(\phi, t)\rangle = \sum_n b_n^l e^{-in\phi} |n\rangle e^{-i\epsilon_l t/\hbar}, \quad (2.10)$$

where, as we shall show in Sec. II C, ϕ is the average value of the phase, the b_n^l are assumed to be real, and the ϵ_l are the junction eigenvalues. If the junction is biased at zero voltage, the b_n^l satisfy the Schrödinger equation

$$\epsilon_l b_n^l = \frac{(2en)^2}{2C} b_n^l - \frac{1}{2} E \cos\phi (b_{n+1}^l + b_{n-1}^l). \quad (2.11)$$

Equation (2.11) is the indicial equation for the well-known Mathieu functions.⁷ There are three limits which are of particular interest.

1. Tight-binding limit: No electrostatic effects

In the limit that $C \rightarrow \infty$, the electrostatic energy required to transfer a pair is zero and the b_n^l satisfy⁸

$$\epsilon_l b_n^l = -\frac{1}{2} E \cos\phi (b_{n+1}^l + b_{n-1}^l). \quad (2.12)$$

Equation (2.12) has two solutions for odd and even parity, respectively,

$$b_n^l = \begin{cases} 0 & \text{for } l=1,3,\dots \\ \text{const} & \text{for } l=0,2,\dots \end{cases} \quad (2.13a)$$

$$(2.13b)$$

so that the (un-normalized) state vector and eigenvalue are

$$|\psi_l(\phi, t)\rangle = \sum_n e^{-in\phi} |n\rangle e^{-i\epsilon_l t/\hbar}, \quad (2.14a)$$

$$\epsilon_l = -E \cos\phi. \quad (2.14b)$$

The state vector, Eq. (2.14a), describes a perfectly phase-ordered state that is not subject to any phase fluctuations. In particular, we note that the fluctuations in the pair number difference $\langle \delta \hat{n}^2 \rangle = \langle \hat{n}^2 \rangle$ (since $\langle \hat{n} \rangle = 0$) are infinite,

$$\langle \delta \hat{n}^2 \rangle = \sum_n n^2 = \infty \quad (2.15)$$

as the state vector (2.14a) includes all n states. Since $\langle \delta n^2 \rangle$ is infinite it follows that there are no phase fluctuations.

2. Plasma oscillations: Intermediate electrostatic effects

If $\sigma \cos\phi \gg 1$, then the b_n^l reduce to Hermite Gaussians

$$b_n^l = \left[\frac{2/\pi}{\sigma \cos \phi} \right]^{1/4} \left[\frac{1}{2^l l!} \right]^{1/2} \\ \times H_l \left[\left[\frac{2}{\sigma \cos \phi} \right]^{1/4} n \right] \\ \times \exp[-n^2/(2\sigma \cos \phi)^{1/2}], \quad (2.16a)$$

$$\epsilon_l = -E \cos \phi + \hbar \omega_p(\phi) \left(l + \frac{1}{2} \right), \quad (2.16b)$$

where

$$\omega_p = \left[\frac{2e}{\hbar C} J \cos \phi \right]^{1/2}$$

is the Josephson plasma frequency.⁹ Note, that as $C \rightarrow \infty$, $\sigma \rightarrow \infty$ and Eqs. (2.16) reduce to the tight-binding limit. Using the virial theorem, we find

$$\langle \delta n^2 \rangle^{1/2} = \left(\frac{1}{2} \sigma \cos \phi \right)^{1/4} \sqrt{2l+1} \quad (2.17)$$

so that the rms phase fluctuations decrease as $\sigma^{-1/4}$.

3. Strong charge fluctuations: Quenching of phase order

If $\sigma \ll 1$, phase coherence across the tunneling barrier is seriously disturbed by electrostatic fluctuations. We can best illustrate the physical nature of this limit by first considering the case $\sigma=0$, where Eq. (2.11) reduces to

$$\epsilon_l b_n^l = \frac{(2en)^2}{2C} b_n^l. \quad (2.18)$$

The ground-state energy eigenvalue in this limit is zero and all of the excited states are doubly degenerate, i.e., we find the following electrostatic energies:

$$\epsilon_n^\pm = \frac{(2en)^2}{2C}, \quad n=0,1,2,\dots \quad (2.19)$$

The ground-state eigenvector $|\psi_0\rangle$ is given by

$$|\psi_0\rangle = |0\rangle, \quad (2.20)$$

and the excited states, denoted by $|\psi_n^\pm(\phi)\rangle$, are

$$|\psi_n^\pm(\phi)\rangle = \frac{1}{\sqrt{2}} (e^{-i\phi} |n\rangle \pm e^{i\phi} |-n\rangle). \quad (2.21)$$

This particular linear combination arises from the requirement that the average pair charge imbalance must be zero, i.e.,

$$\langle \psi_n^\pm | \hat{n} | \psi_n^\pm \rangle = 0. \quad (2.22)$$

We note that the $|\psi_n^+(\phi)\rangle$ are symmetric with

respect to inversion through the origin (in n space) and $|\psi_n^-(\phi)\rangle$ are antisymmetric. If we now turn on the tunneling interaction, but keep $\sigma \ll 1$, pair transfer will split this degeneracy. In particular, using the $|\psi_n^\pm(\phi)\rangle$ notation, the energy eigenvalues are

$$\epsilon_0 = -\frac{1}{2} E \sigma \cos^2 \phi, \quad (2.23a)$$

$$\epsilon_1^- = \frac{2e^2}{C} - \frac{1}{12} E \sigma \cos^2 \phi, \quad (2.23b)$$

$$\epsilon_1^+ = \frac{2e^2}{C} + \frac{5}{12} E \sigma \cos^2 \phi, \quad (2.23c)$$

$$\epsilon_2^\pm = \frac{8e^2}{C} + \frac{1}{15} E \sigma \cos^2 \phi \pm \dots \quad (2.23d)$$

An examination of Eqs. (2.23) reveals the following.

(1) The tunneling interaction splits the doubly degenerate first excited state to second order in $\hat{H}_T \equiv (\hat{H}_T^+ + \hat{H}_T^-)$ with the asymmetric state lying below the symmetric one. Note that the pair-transfer term increases the energy of $|\psi_1^+(\phi)\rangle$, this feature of the junction's eigenspectrum arising from level repulsion. As we shall see in Sec. IV, level repulsion may give rise to surprising thermal characteristics of the dc supercurrent once these states are thermally activated. (2) The second excited state remains doubly degenerate to second order in \hat{H}_T , but is split in fourth order by a term of order $(2e^2/C)(\sigma \cos \phi)^4$. In general, ϵ_n^\pm will be split by a term of order $(2e^2/C)(\sigma \cos \phi)^{n+1}$. (3) As the tunneling interaction is further increased in size and one passes from the strong charge fluctuations to the plasmon regime, the following correspondence can be made between the states $|\psi_n^\pm(\phi)\rangle$ and the Hermite Gaussians, $|\psi_l(\phi)\rangle$,

$$\begin{aligned} |\psi_0^+(\phi)\rangle &\rightarrow |\psi_0(\phi)\rangle, \\ |\psi_1^-(\phi)\rangle &\rightarrow |\psi_1(\phi)\rangle, \\ |\psi_1^+(\phi)\rangle &\rightarrow |\psi_2(\phi)\rangle, \\ |\psi_n^-(\phi)\rangle &\rightarrow |\psi_{l=2n-1}(\phi)\rangle, \\ |\psi_n^+(\phi)\rangle &\rightarrow |\psi_{l=2n}(\phi)\rangle, \end{aligned} \quad (2.24)$$

i.e., the antisymmetric (symmetric) states remain antisymmetric (symmetric). (4) The leading phase-dependent terms of the energy eigenvalues in the limit $\sigma \ll 1$ vary as $E \sigma \cos^2 \phi$. This has a number of interesting consequences regarding the phase and area dependence of the pair current of ultrasmall Josephson junctions as well as its magnetic and thermal characteristics. These aspects of the junction's dynamics are examined in Secs. III and IV.

To see the consequences of electrostatic fluctuations on the coherence properties of the junction, we note that to first order in σ , the ground-state eigenvector is

$$|\psi_0(\phi)\rangle = |0\rangle + \frac{1}{2}\sigma(e^{-i\phi}|1\rangle + e^{+i\phi}|-1\rangle)\cos\phi, \quad (2.25)$$

and the rms number fluctuations are

$$\langle\psi_0(\phi)|\hat{n}^2|\psi_0(\phi)\rangle^{1/2} = \frac{1}{\sqrt{2}}\sigma\cos\phi. \quad (2.26)$$

Equation (2.26) implies that the phase is completely undefined as σ decreases in this limit. Despite the fact that the phase fluctuations are so large, pair transfer is still possible. This aspect of the junction's dynamics will be discussed in Sec. IV.

Figure 1 depicts the rms number fluctuations of the ground state as a function of phase for the specific cases of (1) $\sigma=500$, (2) $\sigma=50$, (3) $\sigma=5$, and (4) $\sigma=\frac{1}{2}$. An examination of this figure reveals the following.

(1) For large values of σ , the rms number fluctuations vary with the pair phase as $(\cos\phi)^{1/4}$, in accordance with Eq. (2.17). Furthermore, near $\phi=0$, the rms number fluctuations decrease as $\sigma^{-1/4}$ as expected.

(2) As ϕ approaches $\pi/2$, the rms number fluctuations rapidly decline to zero indicating that the junction is approaching a definite number state. The decline is most noticeable for devices with large values of σ .

(3) For $\sigma < 1$, the rms number fluctuations rapidly approach a $\sqrt{\cos\phi}$ dependence in accordance with Eq. (2.28).

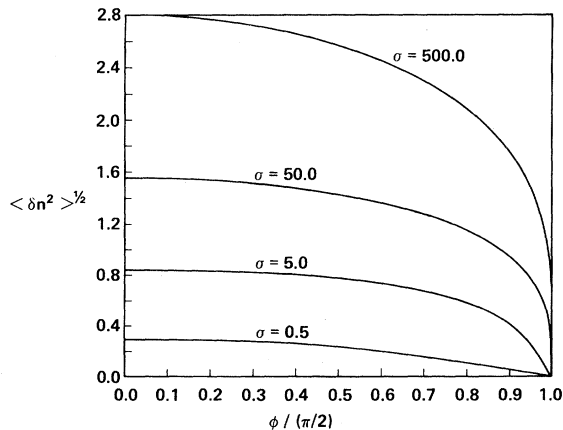


FIG. 1. Phase dependence of the rms number fluctuations at zero temperature for the cases (1) $\sigma=500$, (2) $\sigma=50$, (3) $\sigma=5$, and (4) $\sigma=\frac{1}{2}$.

C. Definite-phase representation

Next, we relate this approach of junction dynamics to standard descriptions which are formulated in the definite-phase representation. We first transform the various operators that appear in the junction Hamiltonian from the definite-number to the definite-phase representation. If the basis vectors in the definite-phase representation are denoted by $|\theta\rangle$, we require $\langle\theta|\hat{Q}|\theta'\rangle$ to obtain the operator \hat{Q} in the definite phase representation. Thus, from Eq. (2.7a), we have for \hat{n}

$$\langle\theta|\hat{n}|\theta'\rangle = \sum_n n \langle\theta|n\rangle \langle n|\theta'\rangle, \quad (2.27)$$

where

$$\langle\theta|n\rangle = e^{-in\theta}. \quad (2.28)$$

Inserting Eq. (2.28) into (2.27), we find

$$\langle\theta|\hat{n}|\theta'\rangle = \delta(\theta-\theta') \left[-i \frac{\partial}{\partial\theta} \right], \quad (2.29)$$

so that, as expected, $n \rightarrow -i(\partial/\partial\theta)$ in the definite-phase representation. For the pair transfer terms, we require

$$\begin{aligned} \langle\theta|\hat{H}_T^\pm|\theta'\rangle &= \frac{1}{2}E \sum_n \langle\theta|n\rangle \langle n\mp 1|\theta'\rangle \\ &= \frac{1}{2}E e^{\pm i\theta} \delta(\theta-\theta'). \end{aligned} \quad (2.30)$$

Thus, the Hamiltonian in the definite-phase representation is

$$H = -\frac{2e^2}{C} \frac{\partial^2}{\partial\theta^2} - E \cos\theta, \quad (2.31)$$

where θ is an operator. The junction wave function in the definite-phase representation is

$$\Psi_l(\theta) = \langle\theta|\Psi_l(\phi)\rangle = \sum_n b_n^l e^{+in(\theta-\phi)}. \quad (2.32)$$

To illustrate the role of ϕ in this context, we recall that the b_n^l are the coefficients of the Mathieu functions of order l . Accordingly, it follows that the eigenfunctions in the definite-phase representation are

$$\psi_{l+}(\theta) = c e_{2l} \left[\frac{\theta-\phi}{2}, -\sigma \cos\phi \right], \quad (2.33a)$$

even symmetry, $l=0,1,2,\dots$

$$\psi_{l-}(\theta) = s e_{2l} \left[\frac{\theta-\phi}{2}, -\sigma \cos\phi \right], \quad (2.33b)$$

odd symmetry, $l=1,2,\dots$

where the $ce_{2l}(\beta, q)$ [$se_{2l}(\beta, q)$] are the even [odd] Mathieu functions of period π which reduce to $\cos 2l\beta$ [$\sin 2l\beta$] in the limit that $q \rightarrow 0$. From Eqs. (2.33) it follows that the wave function is centered at $\theta = \phi$ and has a width set by $(\sigma \cos \phi)^{-1}$. Note that as more current is driven through the junction the wave function broadens in phase space while it narrows in n space. It is instructive to examine limiting forms of Eqs. (2.33) and to use them to calculate the rms phase fluctuations, $\langle \delta \theta^2 \rangle^{1/2} = (\langle \theta^2 \rangle - \phi^2)^{1/2}$.

1. Tight-binding limit: No electrostatic fluctuations

As $\sigma \rightarrow \infty$

$$\psi_{l+}(\theta) \rightarrow \delta(\theta - \phi), \quad (2.34a)$$

$$\psi_{l-}(\theta) \rightarrow 0, \quad (2.34b)$$

and

$$\langle \delta \theta^2 \rangle^{1/2} = 0. \quad (2.35)$$

2. Plasma oscillations: Intermediate electrostatic effects

If $\sigma \cos \phi \gg 1$,

$$\begin{aligned} \psi_l(\theta) \rightarrow & \left[\frac{\alpha}{(\pi 2^l l!)^{1/2}} \right]^{1/2} H_l(\alpha(\theta - \phi)) \\ & \times e^{-[\alpha(\theta - \phi)]^2/2} \end{aligned} \quad (2.36)$$

where $\alpha \equiv (\frac{1}{2} \sigma \cos \phi)^{1/4}$. Furthermore, the rms phase fluctuations are

$$\langle \delta \theta^2 \rangle^{1/2} = (\frac{1}{2} \sigma \cos \phi)^{-1/4} (l + \frac{1}{2})^{1/2}, \quad (2.37)$$

which increases as more current is driven through the junction.

3. Strong charge fluctuations: Quenching of phase order

If $\sigma \cos \phi = 0$,

$$\psi_{l+}(\theta) = \cos l(\theta - \phi), \quad (2.38a)$$

$$\psi_{l-}(\theta) = \sin l(\theta - \phi), \quad (2.38b)$$

and

$$\langle \delta \theta^2 \rangle = \begin{cases} \pi^2/3 & \text{if } l=0 \\ \pi^2/3 + 1/2l^2 & \text{if } l=2, 4, \dots \\ \pi^2/3 - 1/2l^2 & \text{if } l=1, 3, \dots \end{cases} \quad (2.39)$$

so that the phase is undefined in the sense that $\langle \delta \theta^2 \rangle^{1/2}$ is on the order of the range over which θ may vary. The extension to $0 < \sigma \cos \phi \ll 1$ is clear.

Table I summarizes the properties of the ground-state wave function in the definite-number and definite-phase representations.

D. The external circuit

Although the discussion above demonstrates that ϕ is the average value of the Josephson phase, in the sense that

$$\langle \theta \rangle \equiv \int_0^{2\pi} \frac{d\theta}{2\pi} \theta |\psi(\theta)|^2 = \phi, \quad (2.40)$$

TABLE I. Properties of the ground-state wave function in the definite-number and -phase representations.

	Tight-binding limit	Plasma oscillations	Strong charge fluctuations
Wave function in the definite-number representation	$\psi_0(n) = e^{in\phi}$	$\psi_0(n) = \left[\frac{1}{\alpha \sqrt{\pi}} \right]^{1/4} e^{-(n/\alpha)^2/2}$	$\psi_0(n) = \delta_{n,0}$
Wave function in the definite-phase representation	$\psi_0(\theta) = \delta(\theta - \phi)$	$\psi_0(\theta) = \left[\frac{\alpha}{\sqrt{\pi}} \right]^{1/2} e^{-[\alpha(\theta - \phi)]^2/2}$	1
$\langle \delta n^2 \rangle$	∞	$\frac{1}{2} \alpha^2$	0
$\langle \delta \theta^2 \rangle$	0	$\frac{1}{2\alpha^2}$	$\pi^2/3$

we have not yet shown that ϕ is determined by the external drive circuit through the Josephson current-phase relationship. Accordingly, we first review a model of the external drive circuit which shows that ϕ is fixed through the relationship

$$I_W = I(\phi), \quad (2.41)$$

where I_W is the current driven through the junction by the external circuit and $I(\phi)$ is the Josephson current.

In Ref. 4 we presented a model of the external drive circuit for a current-biased Josephson junction. Within this model, we found that the eigenvalue problem reviewed above is unchanged by the external circuit and that ϕ was fixed by Eq. (2.14).

$$\begin{aligned} \dot{\rho}_{n,n'} = & \frac{i}{\hbar} \left[\frac{(2en)^2}{2C} \rho_{n,n'} - \frac{1}{2} E (\rho_{n-1,n'} + \rho_{n+1,n'}) \right] + \frac{1}{\hbar} \left[\frac{(2en')^2}{2C} \rho_{n,n'} - \frac{1}{2} E (\rho_{n,n'-1} + \rho_{n,n'+1}) \right] \\ & - \left(\frac{1}{2} E \right)^2 A (\rho_{n,n'} - \rho_{n-1,n'-1}). \end{aligned} \quad (2.44)$$

Following the approach taken in the eigenvalue problem, we set

$$\rho_{n,n'} = e^{-i(n-n')\phi} \sigma_{n,n'}, \quad (2.45)$$

where $\sigma_{n,n'}$ is real. Inserting Eq. (2.45) into (2.44), equating real and imaginary parts, yields

$$0 = -\frac{i}{\hbar} \left[\frac{(2en)^2}{2C} \sigma_{n,n'} - \frac{1}{2} E \cos\phi (\sigma_{n-1,n'} + \sigma_{n+1,n'}) \right] + \frac{i}{\hbar} \left[\frac{(2en')^2}{2C} \sigma_{n,n'} - \frac{1}{2} E \cos\phi (\sigma_{n,n'-1} + \sigma_{n,n'+1}) \right] \quad (2.46a)$$

and

$$\left(\frac{1}{2} E \right)^2 A (\sigma_{n,n'} - \sigma_{n-1,n'-1}) = \frac{1}{2} E (\sigma_{n-1,n'} - \sigma_{n+1,n'} + \sigma_{n,n'-1} - \sigma_{n,n'+1}) \sin\phi. \quad (2.46b)$$

Equation (2.46a) is just the sum of the Schrödinger equation (2.11) minus its complex conjugate and therefore contains no new information. However, Eq. (2.46b) is new and as we shall demonstrate is the current equation. In particular, we note that

$$\begin{aligned} I_W = 2e \langle \hat{n} \rangle_W &= 2e \sum_n n \langle \dot{\rho}_W \rangle_{n,n} \\ &= 2eA \left(\frac{1}{2} E \right)^2. \end{aligned} \quad (2.47)$$

Setting $n = n'$ in Eq. (2.46b), then multiplying by and summing over n yields

$$I_W = J \sum_n b_n (b_{n+1} - b_{n-1}) n \sin\phi, \quad (2.48)$$

where we have used the fact that $\sigma_{n,n'} = b_n b_{n'}$. Rewriting Eq. (2.48) we have

$$I_W = \frac{1}{2} J \sin\phi \sum_n b_n (b_{n+1} + b_{n-1}). \quad (2.49)$$

Since the circuit is an external system that drives the junction, we use a nonequilibrium density-matrix approach. The density matrix satisfies the operator equation

$$\dot{\hat{\rho}} = -\frac{i}{\hbar} [\hat{H}, \hat{\rho}] + \hat{\rho}_W, \quad (2.42)$$

where

$$\hat{\rho}_W = -\frac{1}{2} A (\hat{H}_T^- \hat{H}_T^+ \hat{\rho} + \hat{\rho} \hat{H}_T^- \hat{H}_T^+ - 2 \hat{H}_T^+ \hat{\rho} \hat{H}_T^-), \quad (2.43)$$

with A set by the current driven through the junction. Within the definite-number representation, Eq. (2.42) is

However, the current operator \hat{I} is defined by

$$\hat{I} \equiv 2e\hat{n} = \frac{2ie}{\hbar} (\hat{H}_T^+ - \hat{H}_T^-), \quad (2.50)$$

and it is easy to show that $\langle \hat{I} \rangle$ is given by the right-hand side of Eq. (2.49), which proves Eq. (2.41).

Next, we extract Anderson's model from our Eq. (2.44). Working in the definite-phase representation, Eq. (2.44) becomes

$$\begin{aligned} \dot{\rho}(\theta, \theta') = & -\frac{i}{\hbar} \left[-\frac{2e^2}{C} \frac{\partial^2}{\partial \theta^2} - E \cos\theta \right] \rho(\theta, \theta') \\ & + \frac{i}{\hbar} \left[-\frac{2e^2}{C} \frac{\partial^2}{\partial \theta'^2} - E \cos\theta' \right] \rho(\theta, \theta') \\ & - \frac{I_W}{2e} (1 - e^{+i(\theta - \theta')}) \rho(\theta, \theta'). \end{aligned} \quad (2.51)$$

Now, if the junction is not driven too far from equilibrium, i.e., both θ and $\theta' \ll \pi/2$, Eq. (2.51) may be written as

$$\begin{aligned} \dot{\rho}(\theta, \theta') = & -i/\hbar \left[-\frac{2e^2}{C} \frac{\partial^2}{\partial \theta^2} - E \cos \theta \right. \\ & \left. - \frac{\hbar I_W}{2e} \theta \right] \rho(\theta, \theta) \\ & + i/\hbar \left[-\frac{2e^2}{C} \frac{\partial^2}{\partial \theta'^2} - E \cos \theta' \right. \\ & \left. - \frac{\hbar I_W}{2e} \theta' \right] \rho(\theta, \theta'), \end{aligned} \quad (2.52)$$

where $\cos \theta \simeq 1 - \theta^2/2$. However, Eq. (2.52) is equivalent to

$$\hat{\rho} = (i/\hbar) [\hat{H}', \hat{\rho}], \quad (2.53)$$

where, in the definite-phase representation

$$\begin{aligned} H' = & -\frac{2e^2}{C} \frac{\partial^2}{\partial \theta^2} - E \cos \theta - \frac{\hbar I_W}{2e} \theta \\ \equiv & H - \frac{\hbar I_W}{2e} \theta, \end{aligned} \quad (2.54)$$

which is just Anderson's phenomenological model of the external circuit.¹⁰ We note that Eqs. (2.53) and (2.54) are strictly valid only when θ is small. Note too, that in this limit $\cos \theta \simeq 1 - \theta^2/2$ so that Eq. (2.54) is the Hamiltonian of a shifted harmonic oscillator, i.e., to within a constant

$$H' = \frac{2e^2}{C} \frac{\partial^2}{\partial \theta^2} - \frac{1}{2} E (\theta - \phi)^2 \quad (2.55)$$

where $\phi = I_W/J$. The eigenfunctions of (2.55) are then shifted Hermite Gaussians in agreement with Eq. (2.36).

Suppose now that we assume Eq. (2.54) is always valid and let us examine the consequences of such an assumption. In particular, if we transform H' back into the definite-number representation, we find

$$H' = H - i \left[\frac{\hbar I_W}{2e} \right] \frac{\partial}{\partial n}. \quad (2.56)$$

Equation (2.56) implies that n is a continuous variable. Now, for large junctions where $E \cos \phi \gg 2e^2/C$, one may treat n as a continuous variable, which generates the harmonic oscillator solutions, i.e., Eqs. (2.16). In fact, as expected, one can show that the eigenfunctions of Eq. (2.56) are

$$\psi_0(n) = b_n^I e^{-in\phi}, \quad (2.57)$$

where the b_n^I are given by Eq. (2.16a) and $\phi \ll \pi/2$. However, suppose we consider an ultrasmall junction in which $E \cos \phi \sim 2e^2/C$. Then, as seen in Eq. (2.25), since the state vector consists of only a few definite-number states, n cannot be treated as a continuous variable and one should use Eq. (2.44) to treat the external circuit. It is for this reason that it is unlikely that the Anderson model of the drive circuit can be directly applied to ultrasmall Josephson junction.

E. Analogy to a rigid rotor in a dc electric field

Recently, Silverman¹¹ obtained the exact eigen-spectrum and eigenfunctions of a two-dimensional rigid rotor in a dc electric field. These solutions are formally identical to those that describe the dc Josephson effect, and there exists an interesting analogy between these two systems.

For convenience, we first follow Silverman and recall that the Hamiltonian for a two-dimensional rigid rotor with moment of inertia I and electric dipole moment \vec{p} in a static uniform electric field $f\hat{x}$ (normal to the angular momentum) is

$$\hat{H} = \frac{\hat{L}_z^2}{2I} - \vec{p} \cdot \vec{f}. \quad (2.58)$$

In the coordinate representation, the Schrödinger equation is

$$\left[-\frac{\hbar^2}{2I} \frac{\partial^2}{\partial \theta^2} - pf \cos \theta \right] \psi_l(\theta) = \epsilon_l \psi_l(\theta) \quad (2.59)$$

and as noted by Silverman, the solutions of Eq. (2.59) are the Mathieu functions. Specifically, the solutions with even symmetry, i.e.,

$$\psi(\theta + 2\pi) = \psi(\theta), \quad (2.60)$$

are

$$\psi_{m+}(\theta) = ce_{2m}(\phi/2, -\sigma), \quad m = 0, 1, 2, \dots \quad (2.61)$$

where $\sigma = pf/(\hbar^2/2I)$. Solutions of odd symmetry, i.e.,

$$\psi(\theta + 2\pi) = -\psi(\theta), \quad (2.62)$$

are

$$\psi_{m-}(\theta) = se_{2m}(\theta/2, -\sigma), \quad m = 1, 2, \dots \quad (2.63)$$

Before making a detailed comparison, we first

cast the above discussion in a language analogous to Eqs. (2.4)–(2.11). Let $|M\rangle$ denote a basis vector of angular momentum $\hbar M$. Then, the rotational energy $\hat{H}_R = \hat{L}_Z^2/2I$ can be written as

$$\hat{H}_R = \frac{\hbar^2}{2I} \hat{M}^2 = \sum_M \frac{\hbar^2 M^2}{2I} |M\rangle \langle M| \quad (2.64)$$

and the coupling to the electric field is

$$\begin{aligned} \hat{H}_E &= \frac{1}{2} pf \sum_M (|M\rangle \langle M+1| + |M-1\rangle \langle M|) \\ &= -(\hat{H}_E^+ + \hat{H}_E^-). \end{aligned} \quad (2.65)$$

A convenient representation for the rotor's eigenvector is

$$|\psi_l(t)\rangle = \sum_M b_M^l |M\rangle e^{-i\varepsilon_l t/\hbar}. \quad (2.66)$$

Inserting Eq. (2.66) into the Schrödinger equation, we obtain

$$\varepsilon_l b_M^l = \frac{\hbar^2 M^2}{2I} b_M^l - \frac{1}{2} pf (b_{M+1}^l + b_{M-1}^l). \quad (2.67)$$

Equation (2.67) is, of course, the indicial equation for the Mathieu function of argument $\sigma = pf/(\hbar^2/2I)$, order l , and is similar to Eq. (2.11) for a Josephson junction in the limit that ϕ is zero. More precisely, we can make the following correspondence: (1) the junction's electrostatic energy and the rotor's rotational energy are entirely analogous, (2) the electric-field–dipole interaction is analogous to the junction's pair transfer term, and (3) the junction's definite-number basis states $|n\rangle$ are analogous to the rigid rotor's basis states $|M\rangle$. Note, however, that there is no analog of the external drive circuit in the rigid-rotor problem as can be seen by comparing Eqs. (2.10) and (2.66). This difference can be further appreciated by recalling that in the definite-phase representation the junction wave functions are

$$\psi_m(\phi) = \begin{cases} ce_{2m} \left[\frac{\theta - \phi}{2}, -\sigma \cos \phi \right] \\ se_{2m} \left[\frac{\theta - \phi}{2}, -\sigma \cos \phi \right] \end{cases} \quad (2.68)$$

for even and odd solutions, respectively. A more detailed understanding can be obtained by examining a number of useful limits.

1. Tight-binding limit: No rotational effects

In the limit that $I \rightarrow \infty$,

$$b_M^l \rightarrow \text{const}, \quad (2.69)$$

independent of M if $l=0, 2, \dots$ so that

$$|\psi_l\rangle \rightarrow \sum_{M=-\infty}^{\infty} |M\rangle. \quad (2.70)$$

Hence in the coordinate representation the eigenfunction and eigenenergy are

$$\psi_l(\theta) = \delta(\theta), \quad (2.71a)$$

$$\varepsilon_l = -pf. \quad (2.71b)$$

In this limit, the rotor is too massive to rotate and the dipole is aligned parallel to the electric field. This is entirely analogous to the tight-binding limit of a Josephson junction in which there are no electrostatic fluctuations and the phase is fixed at $\theta = \phi$.

2. Small oscillations: Weak rotational effects

If $\sigma \gg 1$, basis states with very large M will contribute to the eigenvector and M can be treated as a continuous variable. Approximating

$$b_{M\pm 1}^l \rightarrow b_M^l \pm \frac{\partial}{\partial M} b_M^l + \frac{1}{2} \frac{\partial^2}{\partial M^2} b_M^l$$

we obtain the equation for a harmonic oscillator with

$$\begin{aligned} b_M^l &= \left[\left(\frac{2}{\pi\sigma} \right)^{1/2} \frac{1}{2^l l!} \right]^{1/2} H_l((2/\sigma)^{1/4} M) \\ &\times e^{-M^2/\sqrt{2\sigma}}, \end{aligned} \quad (2.72a)$$

$$\varepsilon_l = -pf + \hbar\omega_R \left(l + \frac{1}{2} \right), \quad (2.72b)$$

where $\omega_R = (pf/I)^{1/2}$. In this limit, the orientational energy is so large compared to the rotational energy, that the rotor is constrained to carry out small oscillations of frequency ω_R about $\theta=0$. This is analogous to the plasmon regime of a Josephson junction in which weak electrostatic effects give rise to small amplitude plasma oscillations about $\theta = \phi$ at a frequency ω_p .

3. Weak-coupling limit: Quadratic Stark effect

If $\sigma \ll 1$, the molecule will be almost freely rotating, and the field will induce only a weak quadratic

Stark effect in the rotor's eigenspectrum. The ground-state and low-lying level spectrum is given by, to lowest order in σ ,

$$\epsilon_0 = -\frac{1}{2}pf \left[\frac{pf}{\hbar^2/2I} \right], \quad (2.73a)$$

$$\epsilon_1^- = \frac{4\hbar^2}{2I} - \frac{1}{12}pf \left[\frac{pf}{\hbar^2/2I} \right], \quad (2.73b)$$

$$\epsilon_1^+ = \frac{4\hbar^2}{2I} + \frac{5}{12}pf \left[\frac{pf}{\hbar^2/2I} \right], \quad (2.73c)$$

$$\epsilon_2^\pm = \frac{16\hbar^2}{2I} + \frac{1}{15}pf \left[\frac{pf}{\hbar^2/2I} \right]. \quad (2.73d)$$

The ground-state eigenvector consists of the $M=0$ state plus a small mixture of the $M=\pm 1$ states, i.e.,

$$|\psi_0\rangle = |0\rangle + \frac{pf}{\hbar^2/I} (|1\rangle + |-1\rangle) + \dots \quad (2.74)$$

Thus, the strong charge fluctuations limit in a Josephson junction is formally equivalent to the quadratic Stark effect exhibited by a two-dimensional rotor.

Next, we note that the dc electric field induces an additional dipole moment p_l in the rotor, given by

$$p_l(f) = -\frac{\partial}{\partial f} \epsilon_l(f). \quad (2.75)$$

In the weak-coupling limit, we find

$$p_0 = p\sigma, \quad (2.76a)$$

$$p_1^- = \frac{1}{6}p\sigma, \quad (2.76b)$$

$$p_1^+ = -\frac{5}{6}p\sigma, \quad (2.76c)$$

$$p_2^\pm = -\frac{2}{15}p\sigma. \quad (2.76d)$$

Note the sign change exhibited by the higher excited rotational states. This feature of the rotor's dynamics arises from and reflects its energy-level structure in the limit that $f \rightarrow 0$. In the next section, we show that the normalized current amplitudes $A_l \equiv I_l/(J \sin\phi)$ are analogous to the induced dipole moments p_l and are given by

$$A_l = -\frac{\partial}{\partial f} \epsilon_l(f) \quad (2.77)$$

where $f = E \cos\phi$. Accordingly, in the strong charge-fluctuation regime, we expect the normalized current amplitudes will exhibit a behavior analogous to Eqs. (2.76).

4. Zero-field limit: Free rotations

In the limit that $f \rightarrow 0$, the eigenvalues reduce to the free rotational spectrum, i.e.,

$$\epsilon_M^\pm = \frac{\hbar^2 M^2}{2I}, \quad (2.78)$$

which is entirely analogous to Eq. (2.19), i.e., the electrostatic energies ϵ_n^\pm . If we choose rotational states, such that $\langle \hat{M} \rangle = 0$, then the eigenvectors $|\psi_M^\pm\rangle$ are given by

$$|\psi_M^\pm\rangle = \frac{1}{\sqrt{2}} (|M\rangle \pm |-M\rangle), \quad (2.79)$$

which is similar to Eq. (2.21) of a superconducting tunnel junction in the limit that $E \rightarrow 0$. Note that in the coordinate representation, the eigenfunctions are given by

$$\psi_M(\theta) = \begin{cases} \cos M\theta, & M=0,1,2,\dots \\ \sin M\theta, & M=1,2,\dots \end{cases} \quad (2.80)$$

for even and odd solutions, respectively.

Finally, in Tables II and III we have summarized this analogy between a Josephson junction and a rotating dipole in an electric field. The quantities x_n^\pm that appear in Table III are $x_0 = \frac{1}{2}$, $x_1^- = \frac{1}{12}$, $x_1^+ = -\frac{5}{12}$, $x_2^\pm = -\frac{1}{15}$, etc.

III. TUNNELING CHARACTERISTICS OF NORMALIZED CURRENT AMPLITUDES IN ULTRASMALL JOSEPHSON JUNCTIONS

Electrostatic fluctuations will influence the pair-transfer characteristics of different junction states in different ways. In particular, on physical grounds we expect that phase coherence in the higher excited states will be more seriously distorted by electrostatic fluctuations than the ground state. Accordingly, in this section, we examine the pair-transfer characteristics of the individual junction states. In Sec. III A we prove that the pair current associated with the state $|\psi_l\rangle$ can be extracted from the energy eigenvalues via the relationship

$$I_l(\phi) = \frac{2e}{\hbar} \frac{\partial}{\partial \phi} \epsilon_l(\phi), \quad (3.1)$$

which is then used to obtain analytic expressions for the current matrix elements in the tight-binding, plasmon, and strong charge-fluctuation limits. We also examine the transition from one regime to another by plotting the variation of the normalized current amplitudes, $A_l(\phi)$, defined by

TABLE II. Analogy of a Josephson junction to a two-dimensional rotor.

Property	Josephson junction	Rotating dipole
Basis vector	$ n\rangle$	$ M\rangle$
Kinetic energy	electrostatic $\frac{(2e\hbar)^2}{2C}$	rotational $\frac{\hat{M}^2}{2I}$
Potential energy	tunneling interaction $-(\hat{H}_T^+ + \hat{H}_T^-)$ $-E \cos\theta$	dipole-field coupling $-\vec{p} \cdot \vec{f}$ $-pf \cos\theta$
Eigenvector $ \Psi_l\rangle$	$\sum_n b_n^l e^{-in\phi} n\rangle$	$\sum_M b_M^l M\rangle$
Eigenfunctions $\psi_l(\theta)$	$ce_{2l} \left[\frac{\theta - \phi}{2}, -\sigma \cos\phi \right]$ $se_{2l} \left[\frac{\theta - \phi}{2}, -\sigma \cos\phi \right]$	$ce_{2l} \left[\frac{\theta}{2}, -\sigma \right]$ $se_{2l} \left[\frac{\theta}{2}, -\sigma \right]$
Induced moment	$A_l = -\frac{\partial \epsilon_l}{\partial f}$	$p_l = -\frac{\partial \epsilon_l}{\partial f}$

$$I_l(\phi) = JA_l(\phi) \sin\phi \quad (3.2)$$

as the electrostatic parameter $\sigma \cos\phi$ varies. In Sec. III B we examine the phase dependence of these am-

plitudes, while in Secs. III C and III D we discuss their scaling and magnetic field characteristics. Finally, in Sec. III E we discuss the thermal characteristics of the normalized current amplitudes.

TABLE III. Analogy of a Josephson junction to a two-dimensional rotor: Behavior in specific regimes.

Regime	Josephson junction	Rotating dipole
Tight-binding limit $\sigma \rightarrow \infty$	no electrostatic effects $C \rightarrow \infty$	no rotational effect $I \rightarrow \infty$
$\psi(\theta)$	$\delta(\theta - \phi)$	$\delta(\theta)$
ϵ	$-E \cos\phi$	$-pf$
Small oscillations $\sigma \gg 1$	plasma oscillations $E \cos\phi \gg 2e^2/C$	rotational oscillations $pf \gg \hbar^2/2I$
$\psi_l(\theta)$	$H_l \left[\left(\frac{\sigma \cos\phi}{2} \right)^{1/2} (\theta - \phi) \right] e^{-(\theta - \phi)^2 [(\sigma \cos\phi)/2]^{1/2}/2}$	$H_L((\sigma/2)^{1/2}\theta) e^{-(\sigma/2)^{1/2}\theta^2/2}$
ϵ_l	$E \cos\phi + \hbar\omega_p(l + 1/2)$	$-pf + \hbar\omega_R(l + \frac{1}{2})$
frequency	$\left[\frac{2e}{\hbar C} J \cos\phi \right]^{1/2}$	$(pf/I)^{1/2}$
Weak coupling $\sigma \ll 1$	strong charge fluctuations $E \cos\phi \ll 2e^2/C$	quadratic Stark effect $pf \ll \hbar^2/2I$
ϵ_n^\pm	$\frac{(2en)^2}{2C} - x_n^\pm E \sigma \cos^2\phi$	$\frac{(\hbar n)^2}{2I} - x_n^\pm \sigma f$
Zero-coupling limit $\sigma = 0$	Non-Josephson junction $E = 0$	free rotor $f = 0$
$\psi_n^\pm(\theta)$	$\cos n(\theta - \phi)$ even solutions $\sin n(\theta - \phi)$ odd solutions	$\cos n\theta$ even solutions $\sin n\theta$ odd solutions
ϵ_n^\pm	$\frac{(2en)^2}{2C}$	$\frac{(\hbar n)^2}{2I}$

A. Anomalous dependence of normalized current amplitudes on $\sigma \cos\phi$

To prove Eq. (3.1), we multiply the indicial equation (2.11) by b_n^l , sum over n , and invoke normalization to obtain

$$\begin{aligned} \epsilon_l = & \sum_n \frac{(2en)^2}{2C} b_n^{l2} \\ & - \frac{1}{2} E \cos\phi \sum_n b_n^l (b_{n+1}^l + b_{n-1}^l). \end{aligned} \quad (3.3)$$

Differentiating with respect to ϕ and rearranging terms, we have

$$\begin{aligned} \frac{\partial \epsilon_l}{\partial \phi} = & \frac{1}{2} E \sum_n b_n^l (b_{n+1}^l + b_{n-1}^l) \sin\phi \\ & + \sum_n \frac{\partial b_n^l}{\partial \phi} \left[\frac{(2en)^2}{C} b_n^l \right. \\ & \left. - E \cos\phi (b_{n+1}^l + b_{n-1}^l) \right]. \end{aligned} \quad (3.4)$$

The second term on the right-hand side of Eq. (3.4) is just

$$2\epsilon_l \sum_n b_n^l \frac{\partial b_n^l}{\partial \phi},$$

which is zero. This leaves

$$\frac{2e}{\hbar} \frac{\partial}{\partial \phi} \epsilon_l = \frac{1}{2} J \sum_n b_n^l (b_{n+1}^l + b_{n-1}^l) \sin\phi, \quad (3.5)$$

which by Eq. (2.45) is the pair current. Next, we examine the pair-current matrix elements in a number of limits.

1. Tight-binding limit: No electrostatic effects

In the tight-binding limit, the energy eigenvalues are given by Eq. (2.18b) so that

$$I_l = J \sin\phi, \quad l=0,2,4,\dots \quad (3.6)$$

Equation (3.6) is just a reflection of the fact that in the tight-binding limit there are no phase fluctuations and the pair current is not reduced by electrostatic fluctuations.

2. Plasma oscillations: Intermediate electrostatic effects

As noted in Sec. II, if $\sigma \cos\phi \gg 1$, electrostatic fluctuations manifest themselves as plasma oscillations¹².

The eigenenergies and pair-current matrix elements (including the lowest-order anharmonic contribution) are given by

$$\begin{aligned} \epsilon_l(\phi) = & -E \cos\phi \left[1 - \left[\frac{2}{\sigma \cos\phi} \right]^{1/2} \left(l + \frac{1}{2} \right) \right] \\ & - \frac{e^2}{2C} \left[\frac{1}{4} + \left(l + \frac{1}{2} \right)^2 \right], \end{aligned} \quad (3.7a)$$

$$I_l(\phi) = J \left[1 - \frac{l + \frac{1}{2}}{(1/2\sigma \cos\phi)^{1/2}} \right] \sin\phi. \quad (3.7b)$$

Note that electrostatic fluctuations suppress the magnitude of the current matrix elements in the upper states to a greater degree than the lower states as expected. Note, too, that the leading anharmonic contribution to the junction energy is of order $1/\sigma$; however, this term is independent of ϕ (in fact it depends only on the junction capacitance) and hence does not modify the pair current. It follows then that the leading anharmonic contribution to the pair-current matrix will be of order $\sigma^{-3/2}$.

3. Strong charge fluctuations: Quenching of phase order

Using Eqs. (3.1) and (2.23) we find to first order in σ

$$I_0(\phi) = \frac{1}{2} J \sigma \sin 2\phi, \quad (3.8a)$$

$$I_1^-(\phi) = \frac{1}{2} J \sigma \sin 2\phi, \quad (3.8b)$$

$$I_1^+(\phi) = -\frac{5}{12} J \sigma \sin 2\phi, \quad (3.8c)$$

$$I_2^\pm(\phi) = -\frac{1}{15} J \sigma \sin 2\phi. \quad (3.8d)$$

An examination of Eqs. (3.8) reveals that the various current matrix elements depend on the Josephson phase as $\sin 2\phi$ instead of $\sin\phi$. Since their magnitudes are proportional to $J\sigma \propto J^2 C$ they scale with junction area as S^3 . Furthermore, in this limit the current matrix elements vary with temperature as $J^2(T)$ instead of $J(T)$.

Table IV summarizes the tunneling characteristics of the normalized current amplitudes in the tight-binding, plasmon, and strong-charge fluctuation regimes. In the tight-binding limit, there are no electrostatic effects, and the normalized current amplitudes are all equal to unity. If the electrostatic parameter is large, but finite, the junction is in the plasmon regime and the normalized current amplitudes are all less than unity. Furthermore, an examination of Table IV reveals that the A_l all exhibit an anomalous phase dependence, as well as modi-

TABLE IV. Anomalous tunneling characteristics of the normalized current amplitudes.

Property	Tight-binding limit	Plasma oscillations	Strong charge Fluctuations
Magnitude	1	$1 - \frac{l + \frac{1}{2}}{\sqrt{(\sigma \cos\phi)/2}}$	$\sigma x_n^\pm \cos\phi$
Scaling characteristics	1	$1 - \frac{l + \frac{1}{2}}{\sqrt{(\cos\phi)/2}} \frac{S_C}{S}$	$\left(\frac{S}{S_C}\right)^2$
Magnetic field	1	$1 - \frac{l + \frac{1}{2}}{\sqrt{\{\sigma[(\text{sink}L)/kL]\cos\phi\}/2}}$	$\frac{\text{sink}L}{kL}$
Thermal characteristics	1	$1 - \frac{l + \frac{1}{2}}{\sqrt{[\sigma f(T)\cos\phi]/2}}$	$f(T)$

fied scaling, magnetic, and thermal characteristics. This feature of junction dynamics reflects the fact that plasma oscillations give rise to phase fluctuations that tend to suppress the degree of phase order between the two superconductors. A particularly appealing way to discuss this regime is to examine the pair-current matrix elements in the definite-phase representation. Thus, in accord with Sec. II C the current operator can be written as

$$I = J \sin(\phi + \delta\theta), \quad (3.9)$$

where $\delta\theta \equiv \theta - \phi$ is the phase fluctuations operator. Since the current in the state $|\psi_l\rangle$ is $\langle \psi_l | I | \psi_l \rangle$, we have

$$A_l = 1 - \frac{1}{2} \langle \psi_l | \delta\theta^2 | \psi_l \rangle, \quad (3.10)$$

where we have used the fact that the wave functions have definite symmetry with respect to $\delta\theta$ in accord with Eq. (2.36) and we are considering only harmonic effects. Application of Eq. (2.37) yields Eq. (3.7b), and it follows that the amplitude of the plasma oscillations sets the size of the phase fluctuations. In particular, any increase in the magnitude of these oscillations further suppresses the pair current. This can be done by either exciting the junction to higher states or "loosening the spring" by decreasing the critical current or the capacitance. An examination of Eqs. (2.37) and (3.7b) reveals that the magnitude of the phase fluctuations increase and the pair current decreases with increasing l or decreasing σ in accord with the discussion above. Furthermore, the scaling, magnetic, and thermal characteristics of the device deviate more sharply from the ideal tight-binding limit as these tendencies are enhanced. If the electrostatic parameter is further decreased, until $\sigma \cos\phi \ll 1$, the junction enters the strong-charge fluctuation regime in which phase order between the two superconductors

is strongly suppressed by electrostatic effects. In this regime, the normalized current matrix elements vary with phase as $\cos\phi$ and scale with junction areas as $(S/S_C)^2$, with magnetic field as $(\text{sink}L/kL)$ and with temperature as $f(T)$. Furthermore, the sign of the A_l of the second and higher excited states is opposite to that of the ground and first excited states. This feature of the junction's dynamics can be understood by recalling the analogy between a Josephson junction and a rotating dipole in a dc electric field. In particular, the pair currents are analogous to the induced dipole moment. This statement is underscored by rewriting Eq. (3.1) as

$$A_l = -\frac{\partial}{\partial f} \epsilon_l(f), \quad (3.11)$$

where the effective electric field $f = E \cos\phi$. Equation (3.11) should be contrasted with the equation for an induced dipole moment, $p_l(f)$, for a molecule in an electric field:

$$p_l = -\frac{\partial}{\partial f} \epsilon_l(f). \quad (3.12)$$

Next, we note that for any system where the level separation increases with excitation, the induced dipole moment is positive for the ground state and negative for all the excited states provided that the matrix elements are all of the same order of magnitude. For the present case the ground state is the lowest level of the symmetric tower of states, and the first excited state is the lowest level of the asymmetric tower of states. As the junction becomes partially phase disordered, these towers gradually take on the character of rotational excitations, and the current matrix elements become negative for all excited states, just as it occurs for the induced dipoles in the quadratic Stark effect.

Figure 2 depicts the dependence of the normal-

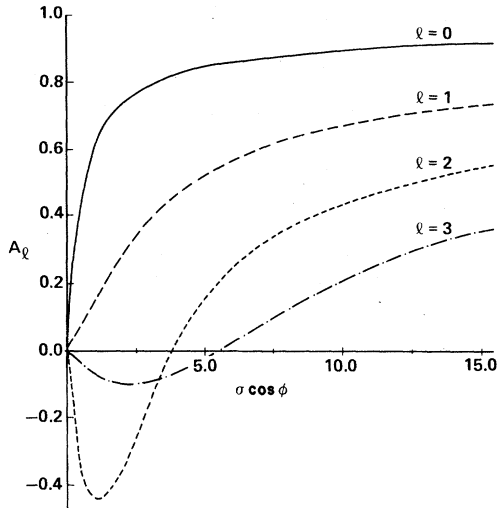


FIG. 2. Dependence of the ground- and first three excited-state normalized current amplitudes on $\sigma \cos \phi$.

ized current amplitudes on the electrostatic parameter $\sigma \cos \phi$ at zero temperature. An examination of this figure reveals the following:

(1) For large values of $\sigma \cos \phi$, the amplitudes vary smoothly with the electrostatic parameter, the ground state varying the slowest and being the largest in accord with Eq. (3.7b).

(2) For $5 < \sigma \cos \phi < 10$, the excited junction state current amplitudes exhibit a much more sensitive dependence on the electrostatic parameter. In particular, $A_3 < 0$ for $\sigma \cos \phi = 5$. Note, however, that the ground-state amplitude still varies only weakly with $\sigma \cos \phi$.

(3) As $\sigma \cos \phi$ continues to decrease, the various current amplitudes exhibit novel behavior. For example, the $l=2$ amplitude switches sign and then becomes very large and negative in the vicinity of $\sigma \cos \phi = 2$. In this same regime, the ground-state amplitude decreases rapidly with $\sigma \cos \phi$, and crossing occurs between A_2 and A_3 in the vicinity of $\sigma \cos \phi = 3$.

(4) For $\sigma \cos \phi < 1$, all of the amplitudes vary linearly with $\sigma \cos \phi$ in accordance with Eqs. (3.8).

B. Phase dependence of normalized current amplitudes

Figure 3 depicts the phase dependence of the ground-state current amplitude for the cases (1) $\sigma = 500$, (2) $\sigma = 50$, (3) $\sigma = 5$, and (4) $\sigma = \frac{1}{2}$. Note the following:

(1) For large values of σ , the ground-state ampli-

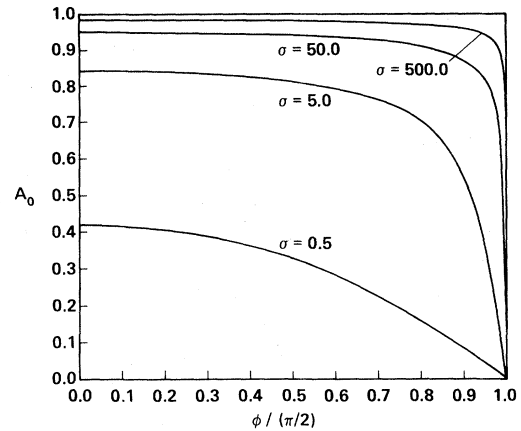


FIG. 3. Phase dependence of the ground-state normalized current amplitude at zero temperature for the cases (1) $\sigma = 500$, (2) $\sigma = 50$, (3) $\sigma = 5$, and (4) $\sigma = \frac{1}{2}$.

tude depends only weakly on ϕ , showing significant phase dependence only in the immediate vicinity of $\phi = \pi/2$. As σ decreases, the range of values of ϕ in which A_0 varies significantly increases.

(2) As σ continues to decrease, the pair-current amplitude decreases in size and exhibits a stronger phase dependence for even small values of ϕ .

(3) For $\sigma = \frac{1}{2}$, A_0 approaches the limiting phase dependence of $\cos \phi$.

Figure 4 depicts the phase dependence of the normalized current amplitudes associated with the ground and first three excited junction states for the case $\sigma = \frac{5}{2}$. Examination of this figure reveals that the ground-state amplitude depends only weakly on the Josephson phase for $\phi \lesssim \pi/4$, varying by about

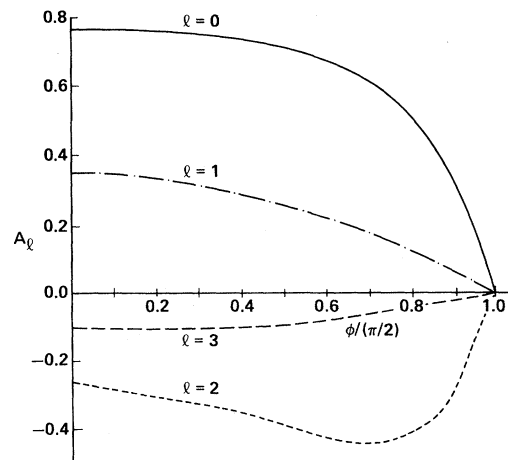


FIG. 4. Phase dependence of the ground- and first three excited-state normalized current amplitudes at zero temperature.

3%. The first excited-state current amplitude depends more sensitively on the Josephson phase, varying by about 11%, in good agreement with Eq. (3.7b). Furthermore, the second and third excited-state current amplitudes vary by 23% and 42%, respectively, in this range. Beyond $\phi = \pi/4$, all of the current amplitudes exhibits a sharper phase dependence. For example, the ground-state current amplitude displays very sensitive phase behavior once ϕ exceeds 86.5° , and the first excited state decreases rapidly for ϕ beyond 78.5° . Furthermore, A_2 and A_3 fall below zero, i.e., the pair currents associated with these states flow in the opposite direction, for ϕ beyond 81° and 77° , respectively.

C. Scaling characteristics of normalized current amplitudes

Figure 5 depicts the scaling characteristics of the normalized current amplitudes for a junction with $S_C = 0.316 \times 10^{-2} \mu\text{m}^2$. For such a device, $\sigma \cos\phi = 10$ when $S = 10^{-2} \mu\text{m}^2$. An examination of this figure reveals the following.

(1) For $S \gg S_C$, the ground-state current amplitude varies only weakly with S in accordance with Table IV. Note, however, that the higher excited-state normalized current amplitudes exhibit a more sensitive area dependence due to their large amplitude plasma oscillations.

(2) As S decreases, the various different normalized current amplitudes exhibit a stronger area dependence. For example, for $S \sim 3S_C$, A_3 switches sign as does A_2 for $S \sim 2.5S_C$. Note that A_2 reaches

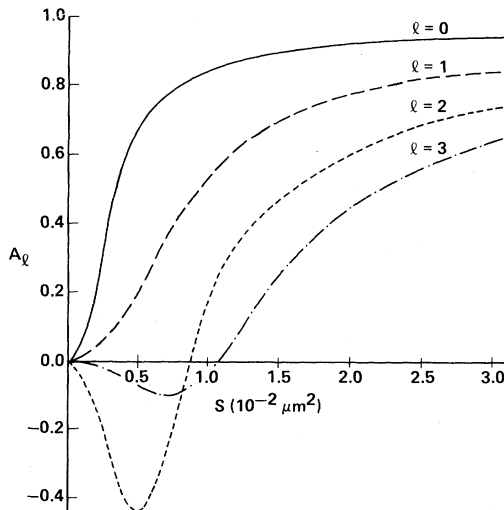


FIG. 5. Scaling characteristics of the ground- and first three-excited state normalized current amplitudes for a junction with $S_C = 4.5 \times 10^{-2} \mu\text{m}^2$.

a relatively large negative value in the vicinity of $2S_C$.

(3) For $S \lesssim 2S_C$, the ground-state current amplitude decreases very rapidly with decreasing junction area.

(4) Finally, for $S < S_C$, the various current amplitudes scale as S^2 in accord with Table IV.

D. Magnetic field characteristics of normalized current amplitudes

In the presence of a dc magnetic field H , the tunneling matrix element is decreased via

$$E \rightarrow E' \equiv E \left[\frac{\sin kL}{kL} \right], \quad (3.13)$$

where L is the junction width, $k = 2e(2\lambda_L + t)H/\hbar c$ with λ_L the London penetration depth, and we have assumed identical superconductors for convenience.

As a consequence of Eq. (3.13)

$$\sigma \rightarrow \sigma(kL) \equiv \sigma \left[\frac{\sin kL}{kL} \right] \quad (3.14)$$

and as kL varies from zero to π , the junction can pass from the plasmon to the strong-charge-fluctuation regimes, with marked changes in the dependence of the A_l on applied magnetic field.

Figure 6 depicts the anomalous magnetic field dependence of the normalized current amplitudes of the ground and first two excited states for a junction with $\sigma \cos\phi = 5$. For small values of kL , the ground-state current amplitude varies only weakly with magnetic field until $kL \simeq \pi/2$, at which point it displays a much more sensitive dependence on the

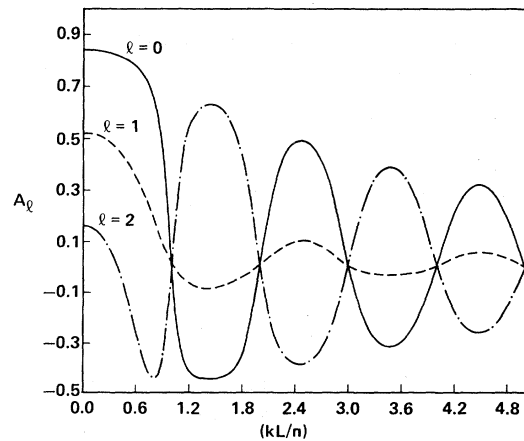


FIG. 6. Anomalous magnetic field characteristics of the ground and first three excited states for a junction with $\sigma \cos\phi = 5$.

amount of flux penetrating the junction. Note the very strong field dependence for $0.9\pi \leq kL \leq 1.1\pi$. Beyond the first lobe in the diffraction pattern, A_0 displays a field dependence that approaches $(\sin kL/kL)$, i.e., the fourth and fifth lobes. Note that the first excited state, which initially assumes the value of $A_1 \simeq 0.54$, rapidly decreases for $kL \gtrsim \pi/2$. Beyond the first lobe, electrostatic effects become so large that they virtually quench the pair current in this state. The second excited junction state is particularly interesting since it assumes an initial value of $A_2 \simeq 0.18$ at $kL=0$. Thus, even for small increases in kL , electrostatic fluctuations are greatly enhanced, and phase order is significantly suppressed in this state.

E. Thermal characteristics of normalized current amplitudes

At finite temperatures, quasiparticle excitations block the pair-transfer process, and this gives rise to a temperature-dependent tunneling matrix element $E(T)$. For identical superconductors

$$E(T) = E(0) \frac{\Delta(T)}{\Delta(0)} \tanh \frac{\Delta(T)}{kT} \equiv E(0)f(T), \quad (3.15)$$

so that as $T \rightarrow T_C$, the critical current amplitude as well as the electrostatic parameter decrease in accordance with Eq. (3.15). Below, we discuss the thermal characteristics of the normalized current amplitudes.

Figure 7 depicts the temperature dependence of the normalized current amplitude for the case $\sigma \cos \phi = 5$. Thus, as T varies from 0 to T_C , the electrostatic parameter varies from 5 to 0, and the junction passes from the plasmon to the strong-charge-fluctuation regime. An examination of this figure reveals that A_0 is virtually independent of temperature, until $T/T_C = 0.8$; for higher temperatures, the ground-state current amplitude varies much more sensitively with T/T_C approaching the limiting functional dependence of Table IV when $1 - T/T_C \simeq 0.01$. The first excited-state normalized current amplitude exhibits a similar behavior, except that it shows appreciable temperature dependence once $T/T_C = 0.7$. The second excited-state normalized current amplitude is almost independent of temperature for $T/T_C \leq 0.4$. It then decreases fairly rapidly with increasing T/T_C and is 0 for $T/T_C = 0.6$. At higher temperatures, A_2 rapidly becomes negative, achieving a minimum value of 0.44

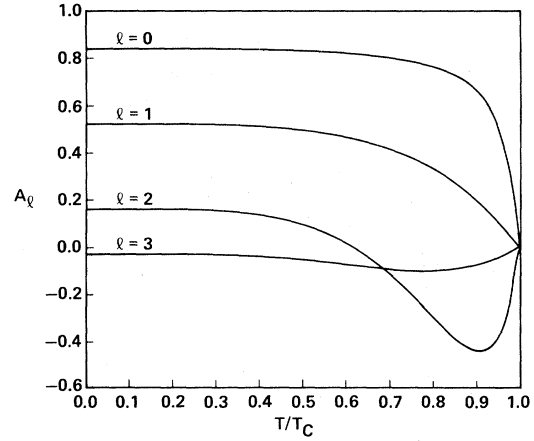


FIG. 7. Anomalous thermal dependence of the ground and first three excited states for a junction with $\sigma \cos \phi = 5$.

at $T/T_C = 0.9$. Beyond this point, it approaches 0 linearly for $1 - T/T_C \lesssim 0.05$. This particular behavior is a reflection of the fact that the higher excited states are more strongly perturbed by electrostatic effects than the lower ones.

IV. TUNNELING CHARACTERISTICS OF THE dc SUPERCURRENT IN ULTRA-SMALL JOSEPHSON JUNCTIONS

In this section, we examine the influence of electrostatic fluctuations on the dc supercurrent when the junction is current based on the zero-voltage dc step. We are particularly concerned with the behavior of the supercurrent when the junction passes from plasmon regime to the strong-charge-fluctuation regime as the electrostatic parameter σ is varied. Accordingly, we examine the tunneling characteristics of the junction for values of σ ranging from 500 down to $\frac{1}{2}$. We note that this corresponds to scaling the device size down from $S = 22.36S_C$ to $S = 0.71S_C$ and renders a fairly complete picture of the pair current's properties.¹³

Since the total supercurrent I is given by

$$I = \frac{1}{Z} \sum_l e^{-\epsilon_l/kT} I_l, \quad (4.1)$$

where

$$Z = \sum_l e^{-\epsilon_l/kT}$$

is the partition function, we anticipate that the junction will exhibit very novel behavior at finite temperature. In particular, we find that the super-

current is a much more sensitive function of temperature in ultrasmall junctions than in larger ones. This feature of ultrasmall devices arises for three reasons.

(1) As T/T_C increases, the electrostatic parameter $\sigma(T)=\sigma(0)f(T)$ decreases, and this can qualitatively effect the supercurrent's tunneling characteristics, especially as the junction passes from the plasmon regime to the strong-charge-fluctuation regime.

(2) The pair-current matrix elements are, for ultrasmall junctions, nonlinear functions of the temperature-dependent critical current amplitude, $J(T)=J(0)f(T)$.

(3) Further, as T/T_C increases, thermal activation of the excited junction states may also occur. Since the pair-current matrix elements of the higher excited junction states have the opposite sign of the lower ones, activation of these states can lead to an additional suppression of the supercurrent.

In Sec. IV A we examine and contrast the tunneling characteristics of the dc supercurrent in the tight-binding, plasmon, and strong-charge-fluctuation regimes. This provides a description of the limiting behavior of the device and serves as a convenient framework for the remainder of Sec. IV, where we discuss the phase dependence, scaling, magnetic, and thermal characteristics of the junction for arbitrary values of σ . In Sec. IV B we discuss the phase dependence of the dc supercurrent as it undergoes the transition from the plasmon to the strong-charge-fluctuation regime. In Secs. IV C and IV D we examine the anomalous scaling and magnetic field dependence of ultrasmall junctions. Finally, in Sec. IV E we discuss the thermal characteristics of ultrasmall Josephson junctions. Of particular interest is the effect of thermal activation of the excited junction states on the tunneling characteristics of the dc supercurrent.

A. Tunneling characteristics of the dc supercurrent in limiting regimes

Table V summarizes the tunneling characteristics of the dc supercurrent in the tight-binding, plasmon, and strong-charge-fluctuation regimes. The quantity $J_C \equiv J(S_C/S)$.

1. Tight-binding limit: No electrostatic effects

Since there are no electrostatic effects in this limit,

$$I = J \sin \phi ,$$

and the supercurrent does not exhibit any anomalous behavior. In particular, the pair current peaks at $\phi = \pi/2$ and scales linearly with the device area. In the presence of a dc magnetic field, the supercurrent exhibits the well-known ($\sin kL/kL$) diffraction pattern and, as shown in Table IV, varies with temperature as $f(T)$, vanishing as $T \rightarrow T_C$.

2. Plasma oscillations: Intermediate electrostatic effects

Using Eqs. (3.7) and (4.1) and ignoring anharmonic terms, we find

$$I(\phi) = J \sin \phi \left[1 - \frac{\coth(\hbar\omega_p/2kT)}{\sqrt{(\sigma \cos \phi)/2}} \right]. \quad (4.2)$$

If $kT \ll \hbar\omega_p$,

$$I(\phi) = J \sin \phi \left[1 - \frac{1}{\sqrt{(\sigma \cos \phi)/2}} \right], \quad (4.3)$$

in this limit the pair current peaks at

$$\cos \phi = \frac{1}{2} \sigma^{-0.2} \quad (4.4)$$

and achieves a value of

$$I \simeq J \left(1 - \frac{5}{8} \sigma^{-0.4} \right). \quad (4.5)$$

Thus for $\sigma = 500$, the current peaks at $\phi = 81.7^\circ$ and is equal to $0.948J$, i.e., plasma oscillations reduce the current by about 5%. An examination of Table IV reveals that the pair current does not scale linearly with area but is quenched by a size-dependent factor $1 - \frac{5}{8}(S_C/S)^{0.8}$ due to zero-point plasma oscillations. The magnetic and thermal characteristics of the junction are also altered by zero-point plasmon effects as shown in Table IV. Note, however, that if an applied magnetic field is tuned so that

TABLE V. Tunneling characteristics of the pair current.

Property	Tight-binding limit	Plasma oscillations	Strong charge
Current-phase relationship			
Ground state	$J \sin\phi$	$\left[1 - \frac{1}{\sqrt{(\sigma \cos\phi)/2}}\right] \sin\phi$	$\sin 2\phi$
Thermal activation	$J \sin\phi$	$\left[1 - \frac{kT}{E \cos\phi}\right] \sin\phi$	$\sin 2\phi$
Phase at maximum current			
Ground state	$\pi/2$	$\cos\phi = \frac{1}{2}\sigma^{-0.2}$	$\pi/4$
Thermal activation	$\pi/2$	$\cos\phi = \left[\frac{kT}{E}\right]^{1/3}$	$\pi/4$
Maximum current			
Ground state	J	$J(1 - \frac{5}{8}\sigma^{-0.4})$	$\frac{1}{2}J\sigma$
Thermal activation	J	$J\left[1 - \frac{3}{2}\left[\frac{kT}{E}\right]^{1/3}\right]$	$\frac{1}{2}J\sigma R(T)$
Diffraction pattern			
Ground state	$\frac{\sin kL}{kL}$	$\frac{\sin kL}{kL} \left[1 - \frac{5/8}{(\sigma \sin kL/kL)^{0.4}}\right]$	$\left[\frac{\sin kL}{kL}\right]^2$
Thermal activation	$\frac{\sin kL}{kL}$	$\frac{\sin kL}{kL} \left[1 - \frac{3}{2}\left[\frac{kT}{E}\right]^{1/3} \left[\frac{\sin kL}{kL}\right]^{-1/3}\right]$	$\left[\frac{\sin kL}{kL}\right]^2$
Scaling characteristics			
Ground state	$J_C \left[\frac{S}{S_C}\right]$	$J_C \left[\frac{S}{S_C}\right] \left[1 - \frac{5}{8} \left[\frac{S_C}{S}\right]^{0.8}\right]$	$\frac{1}{2}J_C \left[\frac{S}{S_C}\right]^3$
Thermal activation	$J_C \left[\frac{S}{S_C}\right]$	$J_C \left[\frac{S}{S_C}\right] \left[1 - \left[\frac{kT}{E(0)}\right]^{1/3} \left[\frac{S_C}{S}\right]^{1/3}\right]$	$\frac{1}{2}J_C \left[\frac{S}{S_C}\right]^3$
Thermal characteristics: $T \rightarrow T_C$			
Ground state	$1 - \frac{T}{T_C}$	$\left[1 - \frac{T}{T_C}\right] \left[1 - \frac{5/8\sigma^{-0.4}}{[(1-T/T_C)]^{0.4}}\right]$	$\left[1 - \frac{T}{T_C}\right]^2$
Thermal activation	$1 - \frac{T}{T_C}$	$\left[1 - \frac{T}{T_C}\right] \left\{ \left[1 - \frac{3}{2} \left[\frac{T/T_C}{E(0)}\right]^{1/3}\right] \left[\frac{T/T_C}{1-T/T_C}\right]^{1/3} \right\} \left[1 - \frac{T}{T_C}\right]^2 R(T)$	

$$\frac{\sin kL}{kL} \lesssim \frac{3.24}{\sigma}, \quad (4.6)$$

In the opposite limit, i.e., $kT \gg \hbar\omega_p$, the current phase relationship is

the junction is no longer in the plasma regime and the system is entering the strong-charge-fluctuation regime. Similarly, once $(T - T_C)/T_C \lesssim 3.24/\sigma(0)$ the device is no longer in the plasma regime and its scaling characteristics deviates significantly from Table V.

$$I = J \sin\phi \left[1 - \frac{kT}{E \cos\phi}\right]. \quad (4.7)$$

In this limit, the pair current peaks at

$$\cos\phi \simeq \left(\frac{kT}{E} \right)^{1/3} \quad (4.8)$$

and achieves a value of

$$I \simeq J \left[1 - \frac{3}{2} \left(\frac{kT}{E} \right)^{1/3} \right]. \quad (4.9)$$

An examination of Table V reveals that the scaling, magnetic, and thermal characteristics of the junction also deviate considerably from the ideal tight-binding limits. In particular, the maximum current does not scale linearly with junction area, but rather deviates by a factor of $1 - a(S_C/S)^{1/3}$, where $a \equiv 1.5[2(kT/\hbar J_C)e]^{1/3}$. Similarly, in the presence of a dc magnetic field, its diffraction pattern departs from the $(\text{sink}L)/kL$ behavior by a factor of $1 - b(kL/\text{sink}L)^{1/3}$ where $b = \frac{3}{2}(kT/E)^{1/3}$. Note that once the magnetic field is tuned so that

$$\frac{\text{sink}L}{kL} \lesssim \frac{27kT}{E} \quad (4.10)$$

the magnetic field characteristics of the supercurrent will depart significantly from Table V as the device will no longer be in the plasmon regime. Finally, when the plasma modes are thermally activated, the pair current scales with temperatures as $f(T)$,

$$1 - \frac{3}{2} \left(\frac{kT}{E(0)} \right)^{1/3} f^{-1/3}(T),$$

so long as

$$\frac{T - T_C}{T_C} < \frac{1}{1 + \frac{8}{27}E/kT_C}. \quad (4.11)$$

If T exceeds this value the device will no longer be in the plasmon regime, and its behavior will deviate considerably from Table V.

3. Strong charge fluctuations: Quenching of phase order

In this limit, there does not appear to be any simple relationships for the total supercurrent at finite

temperatures. At zero temperature

$$I(\phi) = \frac{1}{2} J \sigma \sin 2\phi, \quad (4.12)$$

which approaches a maximum value at $\phi = \pi/4$, being $I = \frac{1}{2} J \sigma$. Thus, a junction with $\sigma = 0.1$ has a maximum current of $0.05J$, and for a device with $C = 10^{-16}$ F, $\sigma = 0.1$, $J = 1.64 \times 10^{-7}$ A, the maximum current will be 8 nA.

At finite temperature, one has

$$I = \frac{1}{Z} \sum_{l=0}^{\infty} e^{-\epsilon_l/kT} I_l(\phi). \quad (4.13)$$

Now, if $2e^2/C \gg E \cos\phi$, to first order in σ

$$I_n^{\pm} = J \sigma x_n^{\pm} \sin 2\phi \quad (4.14)$$

and to the same order, we find for the total current

$$j \sigma \sin 2\phi \frac{\sum_{n=0}^{\infty} x_n^+ e^{-2e^2 n^2/kTC} + \sum_{n=1}^{\infty} x_n^- e^{-2e^2 n^2/kTC}}{1 + 2 \sum_{n=1}^{\infty} e^{-2e^2 n^2/kTC}} f(T) \\ \equiv \frac{1}{2} J \sigma f^2(T) R(T) \sin 2\phi. \quad (4.15)$$

Thus, the current is still a maximum at $\phi = \pi/4$ and is given by

$$I = \frac{1}{2} J \sigma f^2(T) R(T), \quad (4.16)$$

the precise value depending sensitively upon the ratio $(2e^2/C)/kT$.

B. Anomalous phase dependence of the dc supercurrent

Figure 8 depicts the phase dependence of the dc supercurrent for the cases (1) $\sigma = 500$, (2) $\sigma = 50$, (3) $\sigma = 5$, and (4) $\sigma = 0.5$ at zero temperature. Over this range of values the junction makes the transition from the plasmon regime to the strong-charge-fluctuation regime. An examination of this figure reveals the following:

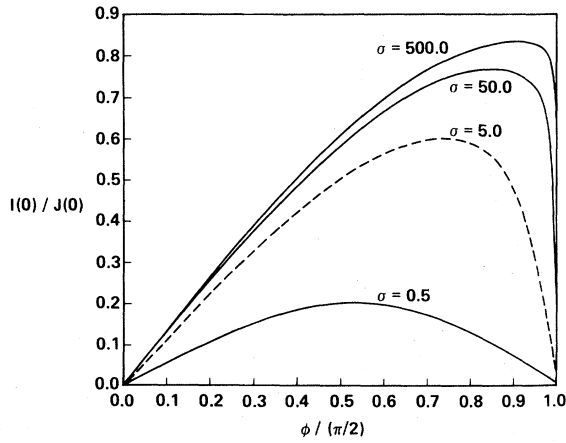


FIG. 8. Phase dependence of the supercurrent at zero temperature for the cases (1) $\sigma=500$, (2) $\sigma=50$, (3) $\sigma=5$, and (4) $\sigma=\frac{1}{2}$.

(1) For $\sigma \gg 1$, the current varies almost sinusoidally with phase until it nears the maximum, at which point it departs from the ideal behavior rather rapidly. Beyond the maximum, the current decreases rapidly with increasing ϕ .

(2) As σ declines, so does the value of the pair phase for which I is a maximum. As $\sigma \rightarrow 0$ this maximum approaches $\pi/4$. For example, at $\sigma = \frac{1}{2}$, the pair current peaks at $\phi = 54^\circ$.

C. Anomalous scaling characteristics of the dc supercurrent

Figure 9 depicts the maximum value of the normalized current amplitude, i.e., I/J , at zero temperature for the specific cases of (1) $S_C = 0.64 \times 10^{-2} \mu\text{m}^2$, (2) $S_C = 0.9 \times 10^{-2} \mu\text{m}^2$, and (3) $S_C = 1.27 \times 10^{-2} \mu\text{m}^2$. An examination of this figure reveals the following:

(1) For $S \gg S_C$, the normalized current increases almost linearly with increasing S , in accord with Table V, which asserts that zero-point plasma oscillations will introduce a factor of $1 - \frac{5}{8}(S_C/S)^{0.8}$ in the supercurrent.

(2) For $S \sim S_C$, the normalized current exhibits an anomalous scaling behavior since the junction is approaching the strong-charge-fluctuation regime. Note that as S_C increases, this behavior tends to flatten out.

(3) For $S \ll S_C$, the normalized current ampli-

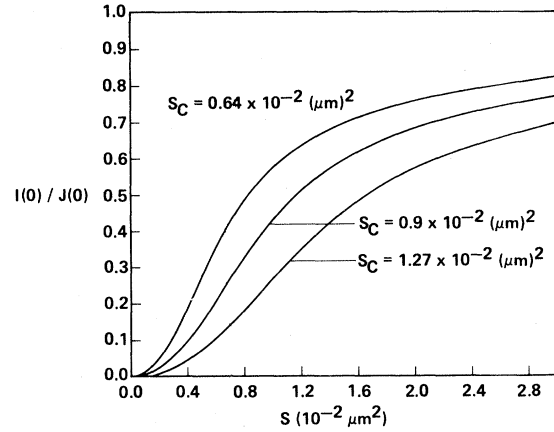


FIG. 9. Anomalous scaling characteristics of I/J at zero temperature for the cases (1) $S_C = 0.64 \times 10^{-2} \mu\text{m}^2$, (2) $S_C = 0.9 \times 10^{-2} \mu\text{m}^2$, and (3) $S_C = 1.27 \times 10^{-2} \mu\text{m}^2$ with the junction biased at maximum current.

tude varies as S^2 , in accord with Table V.

Figure 10 depicts the scaling characteristics of the normalized current amplitude for a junction with $J = 8.8$ (at $T = 0$ K), $l/\epsilon = 1$, and $T_C = 10$ K for the specific cases of (1) $T/T_C = 0$, (2) $T/T_C = 0.5$, (3) $T/T_C = 0.75$, (4) $T/T_C = 0.9$, and (5) $T/T_C = 0.95$. Note that

$$S_C(T) = S_C(0) f^{-1/2}(T), \quad (4.17)$$

so that as T/T_C increases so does $S_C(T)$. Accordingly, we anticipate that as T/T_C increases, the area dependance of the normalized current will tend to flatten out, provided the excited states are not thermally activated. For $S = 3 \times 10^{-14} \text{ m}^2$, the junction capacitance $C \approx 2.7 \times 10^{-16} \text{ F}$ and decreases as $S \rightarrow 0$. For these parameters, the junction is always in the ground state and the scaling characteristics of the device tend to flatten out as $T/T_C \rightarrow 1$.

D. Anomalous magnetic field characteristics of the dc supercurrent

As noted in Sec. III, in the presence of a dc magnetic field

$$\sigma \rightarrow \sigma(kL) = \sigma \left[\frac{\sin kL}{kL} \right].$$

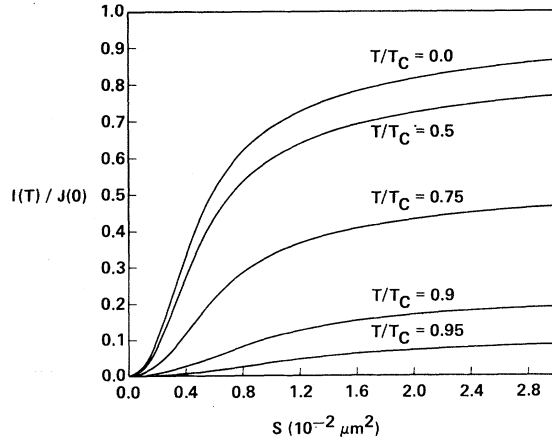


FIG. 10. Anomalous scaling characteristics of $I/J(0)$ for (1) $T/T_C=0$, (2) $T/T_C=0.5$, (3) $T/T_C=0.75$, (4) $T/T_C=0.9$, and (5) $T/T_C=0.95$ for a junction with $S_C(0)=0.45 \times 10^{-2} \mu\text{m}^2$, $T_C=10$ K and the device biased at maximum current.

Thus, by tuning the field toward a diffraction zero, one can probe the influence of electrostatic fluctuations on pair transfer as the junction makes the transition from the plasmon to the strong-charge-fluctuation regime. Below, we present numerical results regarding this transitional behavior.

Figure 11 depicts the zero-temperature anomalous magnetic field dependence of the pair current for the specific cases of (1) $\sigma=500$, (2) $\sigma=50$, (3) $\sigma=5$, and (4) $\sigma=\frac{1}{2}$; i.e., we have plotted

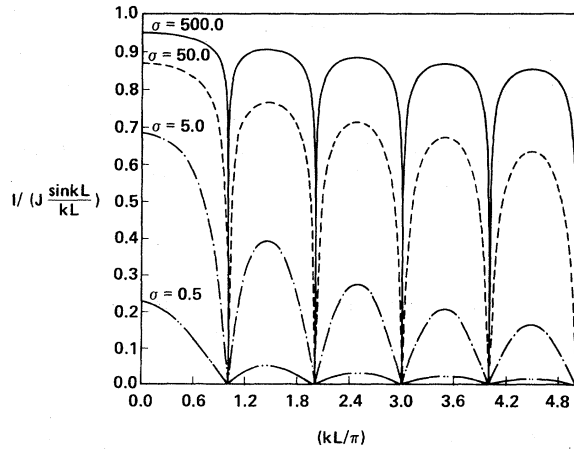


FIG. 11. Anomalous magnetic field dependence $[I/J((\sin kL)/kL)]$ for the cases (1) $\sigma=500$, (2) $\sigma=50$, (3) $\sigma=5$, and (4) $\sigma=\frac{1}{2}$ at zero temperature.

$$A(kL) \rightarrow \frac{I(kL)}{J((\sin kL)/kL)}$$

versus kL/π . An examination of this figure reveals the following.

(1) For large values of S , $A(kL)$ varies only weakly with kL except in the immediate vicinity of the zeros in the diffraction pattern where $A(kL)$ decreases very rapidly. The width of this region increases as S decreases and also with the order of the diffraction lobe.

(2) As σ continues to decrease, $A(kL)$ begins to exhibit significant field dependence for all values of kL . For example, for $\sigma=5$, $A(kL)$ drops by about 8% as kL varies from 0 to $\pi/2$. Tuning the magnetic field towards the diffraction zero further decreases $A(kL)$. Furthermore, the higher lobes in the diffraction pattern are characterized by a significantly varying $A(kL)$.

(3) For $\sigma=\frac{1}{2}$ this trend continues; the higher lobes approach the limiting value of

$$A(kL) \sim \frac{\sin kL}{kL}. \quad (4.18)$$

E. Anomalous thermal characteristics of the dc pair current

From our discussions in Sec. III, it is clear that thermal activation of the excited states will qualitatively alter the junction's tunneling characteristics, especially in the strong-charge-fluctuation regime. Thus, the detailed features of the junction's excitation spectrum are clearly of prime importance in discussing the thermal characteristics of ultrasmall Josephson junctions. Accordingly, we now turn to a discussion of the excitation spectrum of a Josephson junction which is current biased on the zero-voltage dc step.

Figure 12 depicts the excitation spectrum of a Josephson junction normalized by the electrostatic energy, i.e., $(\epsilon_l - \epsilon_0)/(2e^2/C)$ as a function of $\sigma \cos \phi$. An examination of this figure reveals the following:

(1) For large values of $\sigma \cos \phi$, the excitation spectrum is evenly spaced, indicating that the plasma oscillations are harmonic in nature.

(2) As $\sigma \cos \phi$ decreases, the upper states tend to

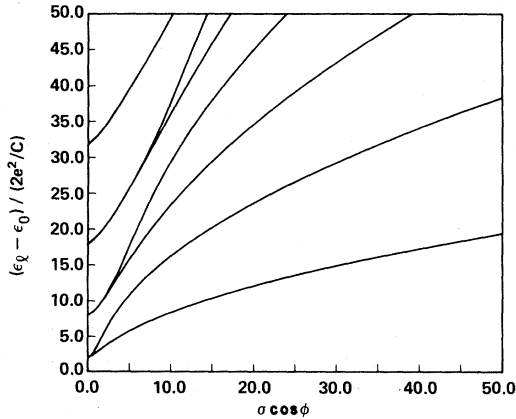


FIG. 12. Excitation spectrum, normalized to $2e^2/C$, as a function of $\sigma \cos \phi$.

become anharmonic, although the lower ones are still reasonably well described via the harmonic oscillator approximation.

(3) As $\sigma \cos \phi$ decreases even further, the higher excited states become doubly degenerate. For example, the fifth and sixth excited states are degenerate when $\sigma \cos \phi \leq 15$, the third and fourth states when $\sigma \cos \phi \simeq 5$.

(4) As $\sigma \cos \phi \rightarrow 0$, the levels approach an electrostatic excitation spectrum.

Below we present numerical results regarding the thermal characteristics of the dc supercurrent and discuss them in reference to Table V.

1. Ground-state effects

Figure 13 depicts the temperature dependence of the normalized current, $A(T) = I(T)/J(T)$, for a junction biased at maximum current with $T_C = 10$ K, $j = 8.8$, and $t/\epsilon = 1$. The cases (1) $\sigma = 500$, (2) $\sigma = 50$, (3) $\sigma = 5$, and (4) $\sigma = \frac{1}{2}$ are considered. For these values, the junction remains in the ground state even for T very close to T_C . An examination of this figure reveals the following.

(1) For large values of σ , the normalized current amplitude is virtually independent of temperature except for a narrow range $\Delta T \equiv T_C - T$ in the immediate vicinity of the transition temperature. Thus, for $\sigma = 500$, $\Delta T/T_C \simeq 0.03$; for $\sigma = 50$, $\Delta T/T_C \simeq 0.05$; however, for $\sigma = 5$, $\Delta T/T_C \simeq 0.15$ and for $\sigma = \frac{1}{2}$, $\Delta T/T_C \simeq 0.35$.

(2) Once T falls within this range, $A(T) \rightarrow 0$ as $T \rightarrow T_C$. For large values of σ , the normalized

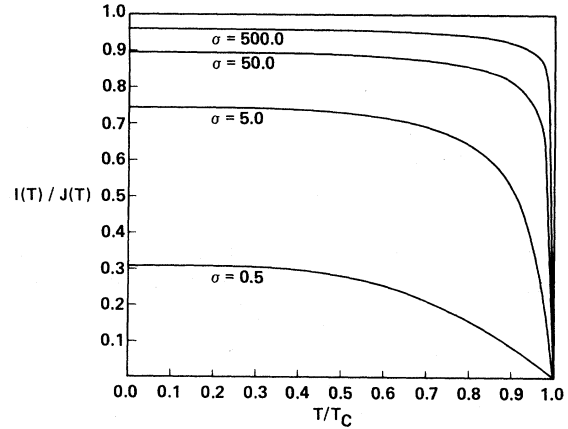


FIG. 13. Temperature dependence of the normalized current amplitude for the cases (1) $\sigma = 500$, (2) $\sigma = 50$, (3) $\sigma = 5$, and (4) $\sigma = \frac{1}{2}$ for a junction with $T_C = 10$ K and a critical current density of 8.8×10^8 A/m².

current falls very rapidly since within this temperature range the junction leaves the plasmon regime and enters the strong-charge-fluctuation regime.

(3) For $\sigma = \frac{1}{2}$, the normalized current decreases linearly with T for $T/T_C \geq 0.8$ in agreement with the limiting behavior depicted in Table V.

Figure 14 depicts the actual temperature dependence of the pair current, i.e., $I(T)/J(0)$, for the same values of the junction parameters.

2. Thermal activation of the excited junction states

We first note that the excitation energy to the first excited state can be written as

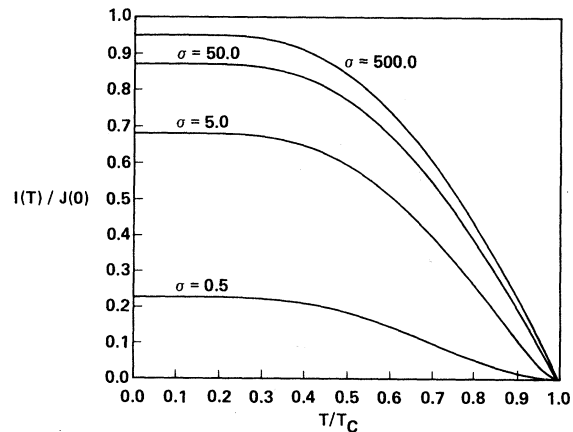


FIG. 14. Temperature dependence of the supercurrent as in Fig. 13.

$$\varepsilon_1 - \varepsilon_0 = \frac{2e^2}{C} G(\sigma), \quad (4.19)$$

where, for example, $G(\sigma)=1$ in the strong-charge-fluctuation regime and $G(\sigma)=\sigma^{0.4}$ in the plasmon regime when the junction is biased at maximum dc current. It follows from Eq. (4.19) that the effect of thermal activation of the excited states on the tunneling characteristics of the supercurrent can be examined by contrasting $I(T)/J(0)$ for junctions with markedly different capacitances, but the same values of σ and T_C at a variety of temperatures.

Figure 15 contrasts the tunneling characteristics of a junction with $C=10^{-16}$ F to one with $C=10^{-15}$ F, both devices having $T_C=10$ K. More precisely, we examine the dependence of $I(T)/J(0)$ on σ for (1) $T/T_C=0.0$, (2) $T/T_C=0.3$, (3) $T/T_C=0.5$, (4) $T/T_C=0.75$, and (5) $T/T_C=0.9$, both junctions being biased at maximum dc current. For the junction with $C=10^{-16}$ F, $2e^2/kC \approx 36.6$ K $> T_C$, so the device is essentially in the ground state for all values of σ . However, for $C=10^{-15}$ F, $2e^2/kC \approx 3.66$ K so that thermal activation of the excited states will play an important role in the junction's dynamics once

$$T = 3.66G(\sigma). \quad (4.20)$$

Note that $\sigma = \sigma(T) = \sigma(0)f(T)$, so that Eq. (4.20) is actually a transcendental equation.

An examination of Fig. 15 reveals that thermal activation of the excited states measurably suppresses the supercurrent for $T/T_C=0.3$ and

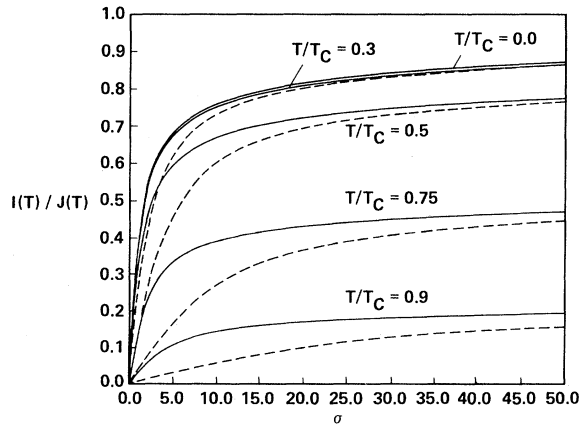


FIG. 15. Dependence of the supercurrent on σ for junctions with $C=10^{-15}$ F (dotted) and $C=10^{-16}$ F (solid) for the cases (1) $T/T_C=0$, (2) $T/T_C=0.3$, (3) $T/T_C=0.5$, (4) $T/T_C=0.75$, and (5) $T/T_C=0.95$.

values of $\sigma \leq 5$ for the junction with $C=10^{-15}$ F. For $T/T_C=0.5$, this effect is noticeable for $\sigma \lesssim 20$. This trend continues as T/T_C increases. For example, for $T/T_C=0.75$, thermal activation of the excited states decreases the supercurrent by a factor of 2 for $\sigma=5$. A similar effect occurs for $T/T_C=0.9$ and $\sigma=20$.

Figure 16 depicts the anomalous magnetic field characteristics for a junction with $J(0)=10^{-17}$ A, $C=4.1 \times 10^{-15}$ F, $\sigma=5$, $T_C=10$ K at $T=0$ and $T=1$ K. For these values of junction parameters, thermal activation of the excited states is substantial by $T=0.9$ K. Note the behavior of the pair current in the vicinity of the diffraction zeros where thermal activation of the excited states is very noticeable. Note, too, the higher diffraction lobes where the pair current at $T=1$ K differs substantially from the zero-temperature curve.

V. CURRENT AND VOLTAGE FLUCTUATIONS ON THE ZERO-VOLTAGE dc STEP

In this section, we examine the current and voltage fluctuations of an ultrasmall Josephson junction that is current biased on the zero-voltage dc step. In contrast to large junctions, where the noise currents are much smaller than the supercurrent, ultrasmall junctions are characterized by noise currents which are often larger than the supercurrent. For these devices, the major sources of current noise are order-disorder fluctuations,¹⁴ which arise from the fact that although

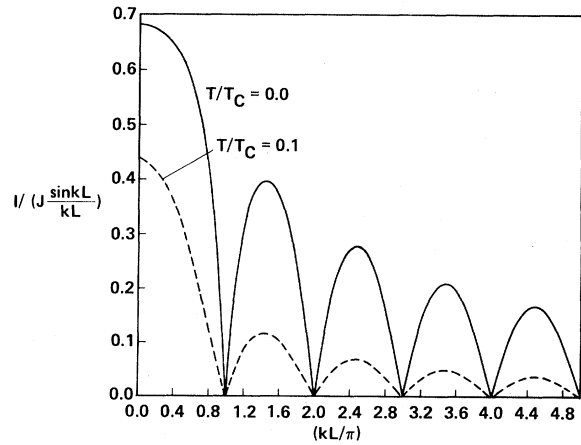


FIG. 16. Anomalous magnetic field characteristics for a junction with $\sigma=5$, $C=4.8 \times 10^{-15}$ F, $T_C=10$ K, and $J(0)=10^{-7}$ A for the cases (1) $T=0$ (solid) and (2) $T=1$ K (dotted).

$\langle \psi_0 | \hat{I} | \psi_0 \rangle$ is of order $J\sigma$ in the strong-charge-fluctuation regime, $\langle \psi_0 | \hat{I}^2 | \psi_0 \rangle^{1/2}$ is of order J . Consequently, the signal-to-noise ratio is of order $\sigma \ll 1$, although this does not necessarily imply that pair currents in the strong-charge-fluctuation regime are unobservable. In particular, we find that the spectrum of current fluctuations are peaked at frequencies in the vicinity of $2e^2/\hbar C$, and this feature of junction dynamics can be exploited to probe the physics of the strong-charge-fluctuation regime.

We also examine voltage fluctuations when the junction is biased on the zero-voltage dc current step. Among other things, we find that the noise voltage peaks in the vicinity of $S \sim S_C$, dropping to 0 as $S \rightarrow \infty$ and $S \rightarrow 0$ provided that the excited states are not thermally activated. We have also examined the spectrum of voltage fluctuations and find that in the strong-charge-fluctuation regime it is dominated by high-frequency components that peak in the vicinity of $2e^2/\hbar C$.

In Sec. V A we examine the tunneling characteristics of the noise current and in Sec. V B we discuss the properties of the current-fluctuation spectrum. In Sec. V C we consider the rms noise voltage $\langle \delta V^2 \rangle^{1/2}$, and in Sec. V D we examine the properties of the voltage-fluctuation spectrum.

A. Noise current

The mean-square current $\langle I_l^2 \rangle$ associated with the l th junction state is given by

$$\langle I_l^2 \rangle = \frac{1}{2} J^2 \sum_n b_n^l [b_n^l - \frac{1}{2}(b_{n+2}^l + b_{n-2}^l) \cos 2\phi], \quad (5.1)$$

so that the total noise current $\langle \delta I^2 \rangle$ is

$$\langle \delta I^2 \rangle = \frac{1}{Z} \sum_l e^{-\epsilon_l/kT} \langle I_l^2 \rangle - I^2. \quad (5.2)$$

Below we present analytic and numerical results regarding the rms noise current, $\langle \delta I^2 \rangle^{1/2}$.

1. Tight-binding limit: No electrostatic effects

In the tight-binding limit, the probability amplitudes are independent of n , so that

$$\langle \delta I^2 \rangle = \frac{1}{2} J^2 (1 - \cos 2\phi) - J^2 \sin^2 \phi = 0. \quad (5.3)$$

Thus, as expected, the rms noise current is zero in the tight-binding limit.

2. Plasma oscillations: Intermediate electrostatic effects

In this regime, n may be treated as a continuous variable, and with the use of the virial theorem, Eq. (5.1) can be written as

$$\langle I_l^2 \rangle = J^2 \sin^2 \phi + \frac{J^2 \cos 2\phi}{\sqrt{(\sigma \cos \phi)/2}} (l + \frac{1}{2}). \quad (5.4)$$

The second term in Eq. (5.4) arises from plasma oscillations. Summing Eq. (5.4) over all plasmon states and subtracting $\langle \hat{I} \rangle^2$, we find the rms noise current to order $\sigma^{-1/4}$:

$$\langle \delta I^2 \rangle^{1/2} = J \sqrt{\cos 2\phi} \left[\frac{\coth^2(\hbar\omega_p/2kT)}{2\sqrt{2\sigma \cos \phi}} \right]^{1/2}. \quad (5.5)$$

If $\hbar\omega_p \gg kT$, the current fluctuations arise primarily from zero-point plasma oscillations, the rms noise current, and signal-to-noise ratio S/N , being given by

$$\langle \delta I^2 \rangle^{1/2} = \frac{J \cos \phi}{(2\sigma \cos \phi)^{3/4}}, \quad (5.6a)$$

$$S/N = (2\sigma \cos \phi)^{1/4} \tan \phi. \quad (5.6b)$$

If the junction is biased at maximum current the rms noise current and the signal-to-noise ratio scale as

$$\langle \delta I^2 \rangle^{1/2} = \frac{1}{2} J_C (S/S_C)^{0.2}, \quad (5.7a)$$

$$S/N = 2(S/S_C)^{0.8}, \quad (5.7b)$$

so that for $S \gg S_C$, the signal-to-noise ratio scales almost linearly with junction area. Furthermore, the thermal characteristics of the rms noise current and the signal-to-noise ratio in this limit are

$$\langle \delta I^2 \rangle_T^{1/2} = \langle \delta I^2 \rangle_0^{1/2} f^{0.6}(T), \quad (5.8a)$$

$$(S/N)_T = (S/N)_0 f^{0.4}(T), \quad (5.8b)$$

provided that the excited states are not thermally activated.

If $kT \gg \hbar\omega_p$, thermal excitation of the plasma oscillations dominates the noise characteristics of the junction and

$$\langle \delta I^2 \rangle^{1/2} = J \cos \phi \left[\frac{kT}{E \cos \phi} \right]^{1/2}, \quad (5.9a)$$

$$\frac{S}{N} = \left[\frac{E \cos \phi}{kT} \right]^{1/2} \tan \phi. \quad (5.9b)$$

If the junction is biased at maximum supercurrent

the rms noise current and the signal-to-noise ratio scale as

$$\langle \delta I^2 \rangle^{1/2} = J_C \left[\frac{kT}{\hbar J_C / 2e} \right]^{5/6} \left[\frac{S}{S_C} \right]^{1/6}, \quad (5.10a)$$

$$\frac{S}{N} = \left[\frac{\hbar J_C / 2e}{kT} \right]^{5/6} \left[\frac{S}{S_C} \right]^{5/6}. \quad (5.10b)$$

Finally, the detailed temperature dependence is

$$\langle \delta I^2 \rangle_T^{1/2} = \frac{J(0)}{[E(0)]^{5/6}} f^{1/6}(T) (kT)^{5/6}, \quad (5.11a)$$

$$\left[\frac{S}{N} \right]_T = \left[\frac{E(0)}{kT} \right]^{5/6} f^{5/6}(T), \quad (5.11b)$$

and in the limit that $T/T_C \rightarrow 1$,

$$\langle \delta I^2 \rangle^{1/2} \rightarrow (1 - T/T_C)^{1/6}, \quad (5.12a)$$

$$S/N \rightarrow (1 - T/T_C)^{5/6}. \quad (5.12b)$$

3. Strong charge fluctuations: Quenching of phase order

In the strong-charge-fluctuation regime,

$$b_n^l b_{n \pm 2}^l \lesssim \sigma^2, \quad (5.13)$$

so that to zero order in $\sigma \ll 1$, we have

$$\langle I_i^2 \rangle = \frac{1}{2} J^2. \quad (5.14)$$

It follows that the rms current noise and signal-to-noise ratio are

$$\langle \delta I^2 \rangle^{1/2} = \frac{1}{\sqrt{2}} J, \quad (5.15a)$$

$$\frac{S}{N} = \frac{1}{\sqrt{2}} \sigma R \sin 2\phi. \quad (5.15b)$$

Thus the rms noise current is independent of phase while the signal-to-noise ratio peaks at $\phi = \pi/4$. The rms noise current scales as S/S_C and varies with temperature as $f(T)$. The signal-to-noise ratio scales as $(S/S_C)^2$ if the excited junction states are not thermally activated and also varies with temperature as $f(T)$. If the excited junction states are thermally activated, the signal-to-noise ratio will be further decreased.

The scaling characteristics of the signal-to-noise ratio are depicted in Fig. 17 for the cases (1) $S_C = 0.64 \times 10^{-2} \mu\text{m}^2$, (2) $S_C = 0.9 \times 10^{-2} \mu\text{m}^2$, and (3) $S_C = 1.27 \times 10^{-2} \mu\text{m}^2$ with the junction biased at maximum current and maintained at zero temperature. Note that the signal-to-noise ratio drops

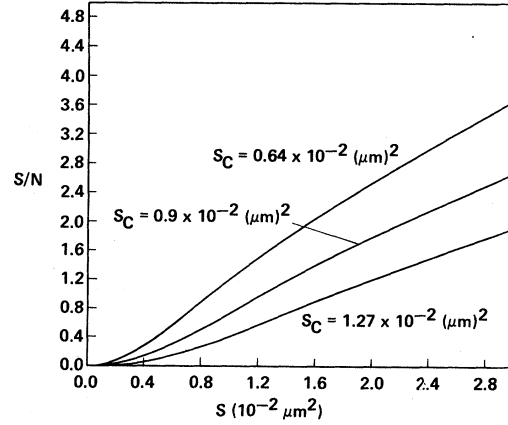


FIG. 17. Scaling characteristics of the signal-to-noise ratio at zero temperature for (1) $S_C = 0.64 \times 10^{-2} \mu\text{m}^2$, (2) $S_C = 0.9 \times 10^{-2} \mu\text{m}^2$, and (3) $S_C = 1.27 \times 10^{-2} \mu\text{m}^2$.

below unity once $S/S_C \leq \frac{4}{3}$. For $S \gg S_C$ S/N scales as $(S/S_C)^{0.8}$, whereas for $S \ll S_C$, the signal-to-noise ratio clearly scales as $(S/S_C)^2$.

Figure 18 depicts the temperature dependence of the signal-to-noise ratio for a junction with $j = 8.8$, $l/\epsilon = 1$, and (1) $\sigma = 500$, (2) $\sigma = 50$, (3) $\sigma = 5$, and (4) $\sigma = 1/2$. For these parameters the excited states are not substantially activated so that the junction is primarily in the ground state. Note that near T_C , S/N scales roughly as $\sqrt{1 - T/T_C}$ in accord with Eq. (5.8b), whereas below $T_C/2$, S/N is almost independent of temperature.

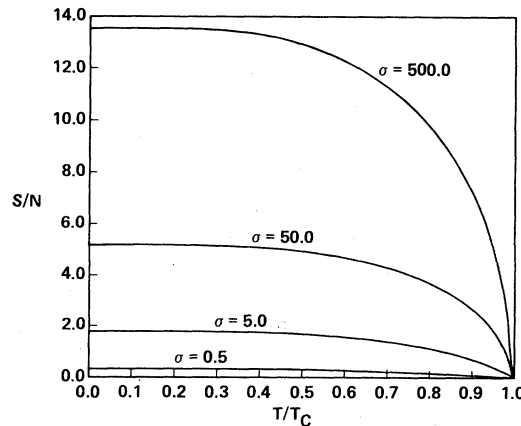


FIG. 18. Temperature dependence of the signal-to-noise ratio for (1) $\sigma = 500$, (2) $\sigma = 50$, (3) $\sigma = 5$, and (4) $\sigma = \frac{1}{2}$ for a junction with $T_C = 10$ K and $j = 8.8$.

B. Power spectrum of current fluctuations

The power spectrum of current fluctuations, $P_I(\omega)$ is given by⁴

$$P_I(\omega) = \sum_{l \neq 0} |\langle \psi_0 | \hat{I} | \psi_l \rangle|^2 g_l(\omega), \quad (5.16)$$

where $g_l(\omega)$ is the normalized line-shape function for the state $|\psi_l\rangle$. For simplicity, we shall assume that $g_l(\omega)$ is a Lorentzian centered at Ω_l with a width $\Gamma_l = \Omega_l/2Q$, where Q is the cavity Q . In that case, the power spectrum of current fluctuations $P_I(\omega)$ is

$$P_I(\omega) = \sum_{l \neq 0} |\langle \psi_0 | \hat{I} | \psi_l \rangle|^2 \frac{\Gamma_l/\pi}{(\omega - \Omega_l)^2 + \Gamma_l^2}. \quad (5.17)$$

1. Tight-binding limit: No electrostatic fluctuations

As noted in Sec. V A, there are no current fluctuations in this limit, so that

$$P_I(\omega) = 0. \quad (5.18)$$

2. Plasma oscillations: Intermediate electrostatic effects

The matrix element of the current, between the states $|\psi_0\rangle$ and $|\psi_l\rangle$ is given by

$$\langle \psi_0 | \hat{I} | \psi_l \rangle = \frac{1}{2} i J \sum_n b_n^0 (b_{n+1}^l e^{-i\phi} - b_{n-1}^l e^{+i\phi}). \quad (5.19)$$

If $l = 1$, Eq. (5.19) becomes

$$\langle \psi_0 | \hat{I} | \psi_1 \rangle = i \frac{J \cos \phi}{(2\sigma \cos \phi)^{1/4}}, \quad (5.20)$$

whereas for $l = 2$

$$\langle \psi_0 | \hat{I} | \psi_2 \rangle = \frac{1}{2^{1/4}} J \sin \phi (\sigma \cos \phi)^{-7/4}, \quad (5.21)$$

Inserting Eqs. (5.20) and (5.21) into (5.17) yields for the spectrum of pair current fluctuations

$$P_I(\omega) = J^2 \left[\frac{\cos^2 \phi}{\sqrt{2\sigma \cos \phi}} g_1(\omega) + \frac{\sin^2 \phi}{\sqrt{2\sigma \cos \phi}} \frac{1}{(\sigma \cos \phi)^3} g_2(\omega) \right]. \quad (5.22)$$

If the junction is biased at maximum current, the leading contribution to the spectrum of current fluctuations is

$$P_I(\omega) = J_C^2 \left[\frac{S}{S_C} \right]^{0.4} \frac{1}{(\omega - \Omega_1)^2 + \Gamma_1^2}. \quad (5.23)$$

If $\hbar\omega_p \gg kT$, the junction remains in the ground state and it scales with temperature as

$$P_I(\omega; T) = J^2 \sigma^{-0.8} f^{1.2}(T) \frac{\Gamma'_1/\pi}{(\omega - \Omega'_1)^2 + \Gamma'^2_1}, \quad (5.24)$$

where Ω'_1 and Γ'_1 are the temperature-dependent transition frequency and lifetime of the first excited state. At maximum current the position of the line center scale as

$$\omega_p(T) = \omega_p(0) f^{0.4}(T) \quad (5.25)$$

and the width as

$$\Gamma_1(T) = \Gamma_1(0) = f^{0.4}(T) \frac{Q(0)}{Q(T)}, \quad (5.26)$$

where the cavity Q is temperature dependent due to quasiparticle excitation.

3. Strong charge fluctuations: Quenching of phase order

To zero order in σ , the ground state is coupled to both the first and second excited state. In particular,

$$\langle \psi_0 | \hat{I} | \psi_n^\pm \rangle = \begin{cases} \frac{1}{\sqrt{2}} i J \cos \phi & \text{if } l = |\psi_1^- \rangle \\ \frac{1}{\sqrt{2}} J \sin \phi & \text{if } l = |\psi_1^+ \rangle \end{cases}. \quad (5.27)$$

Since these states are degenerate, the spectrum of current fluctuations becomes

$$P_I(\omega) = \frac{1}{2} J^2 \frac{\Gamma/\pi}{(\omega - \Omega)^2 + \Gamma^2}, \quad (5.28)$$

where $\hbar\Omega = 2e^2/C$ and we have assumed that the lifetimes of these two states are the same. The spectrum scales with junction area as $(S/S_C)^2$ but also moves to higher frequencies since $\Omega \propto 1/S$ and becomes broader. If $kT \ll 2e^2/C$, the excited junction states will not be thermally activated and the power spectrum will scale with temperature as $f^2(T)$. In addition, it will also broaden due to a de-

crease in cavity Q arising from thermal excitation of quasiparticles.

The frequency structure of Eq. (5.28) can be exploited to probe the physics of the strong-charge-fluctuation regime. In particular, although the signal-to-noise ratio is less than unity in this regime, the current fluctuations are essentially high frequency in nature, peaking at $\omega \sim \Omega$. Accordingly, if a low-pass band filter of bandwidth $\Delta\omega \ll \Omega$ is used, only a fraction of the current fluctuations will be sensed in a measurement of the supercurrent, and the signal-to-noise ratio is

$$\left\langle \frac{S}{N} \right\rangle_{\Delta\omega} = \sqrt{2\pi} Q \sigma R \left[\frac{\Omega}{\Delta\omega} \right]. \quad (5.15b')$$

Thus, for a junction with $\sigma = 0.1$, $Q = 10$, $C = 10^{-16}$ F, and $\Delta\omega = 10^8$ Hz, $(S/N)_{\Delta\omega} = 2.2 \times 10^5 R$ and $R \sim 1$, since thermal excitation of the higher states should not occur for small capacitances. On the other hand, for $C = 10^{-14}$ F, $(S/N)_{\Delta\omega} = 2.2 \times 10^2 R$ so that so long as $R \gtrsim 10^{-2}$ the current in the regime should be observable.

C. Noise voltage

Since the junction is biased at zero voltage, the mean-square noise voltage $\langle \delta V_l^2 \rangle$ associated with the l th state is

$$\langle \delta V_l^2 \rangle = \sum_n \left[\frac{2en}{C} \right]^2 b_n^{l2}. \quad (5.29)$$

Below, we present analytic and numerical results.

1. Tight-binding limit: No electrostatic effects

In the limit that $C \rightarrow \infty$, $\langle \delta V_l^2 \rangle \rightarrow 0$, so there are no voltage fluctuations despite the fact that $\langle \delta n^2 \rangle \rightarrow \infty$.

2. Plasma oscillations: Intermediate electrostatic effects

Using the virial theorem, we have

$$\langle \delta V_l^2 \rangle = \frac{\hbar\omega_p}{C} \left(l + \frac{1}{2} \right), \quad (5.30)$$

and summing over all the junction states yields

$$\langle \delta V^2 \rangle = \frac{\hbar\omega_p}{2C} \coth \frac{\hbar\omega_p}{2kT}. \quad (5.31)$$

If $\hbar\omega_p \gg kT$, zero-point fluctuations dominate the noise and the rms noise voltage is

$$\langle \delta V^2 \rangle^{1/2} = \left[\frac{\hbar\omega_p}{2C} \right]^{1/2}. \quad (5.32)$$

If the junction is biased at maximum current

$$\langle \delta V^2 \rangle^{1/2} = \frac{e}{C} \sigma^{0.2}. \quad (5.33)$$

Thus, the rms noise voltage scales as $\sigma^{0.2}$ and scales with junction area as $S^{-0.6}$. Hence, as $S \rightarrow \infty$, $\langle \delta V^2 \rangle^{1/2} \rightarrow 0$ in agreement with physical intuition. Furthermore, as $C \rightarrow \infty$, the noise voltage vanishes in accord with the tight-binding limit. Note that the noise voltage scales with temperature as $f^{0.2}(T)$, i.e., it decreases with increasing temperature.

If $kT \gg \hbar\omega_p$, the rms noise voltage reduces to the well-known result

$$\langle \delta V^2 \rangle^{1/2} = \left[\frac{kT}{C} \right]^{1/2} \quad (5.34)$$

and scales with junction area as $S^{-1/2}$. In addition, the noise voltage varies with temperature as $T^{0.5}$, i.e., it increases with increasing temperature.

3. Strong charge fluctuations: Quenching of phase order

As $\sigma \rightarrow 0$, the junction enters the strong-charge-fluctuation regime and the eigenfunctions collapse to Eqs. (2.23) and (2.24). In the limit that the electrostatic parameter is zero, the mean-square noise voltage associated with the state $|\psi_n^\pm(\phi)\rangle$ is

$$\langle \psi_n^\pm | \delta V^2 | \psi_n^\pm \rangle = \frac{(2en)^2}{2C}. \quad (5.35)$$

If we now turn on the tunneling interaction, but keep $\sigma \gg 1$, only the ground state is significantly altered from Eq. (5.35) and

$$\langle \psi_0 | \delta V^2 | \psi_0 \rangle = \frac{1}{2} \left[\frac{2e}{C} \right] \sigma^2 \cos^2 \phi. \quad (5.36)$$

Thus, the total mean-square noise voltage

$$\langle \delta V^2 \rangle = \frac{1}{Z} \left[\frac{E \cos \phi}{\sqrt{2e}} \right] + \frac{1}{Z} \sum_n e^{-(2en)^2/2CkT} \frac{(2en)^2}{C}, \quad (5.37)$$

where the sum in Eq. (5.37) includes both symmetric and antisymmetric states. If $kT \ll 2e^2/C$, the excited states are not thermally activated and the rms noise voltage reduces to

$$\langle \delta V^2 \rangle^{1/2} \rightarrow \frac{E \cos \phi}{\sqrt{2}e}. \quad (5.38)$$

If the junction is biased at maximum current, the rms noise voltage is

$$\langle \delta V^2 \rangle^{1/2} = \frac{\hbar J}{(2e^2)}, \quad (5.39)$$

which scales with junction area as S/S_C . For a junction with $J=10^{-7}$ A, the rms noise voltage is 1.95×10^{-4} V. Furthermore, at finite temperatures

$$\langle \delta V^2 \rangle_T^{1/2} = \langle \delta V(0) \rangle^{1/2} f(T), \quad (5.40)$$

which vanishes at $T/T_C \rightarrow 1$. Finally, we note that so long as $kT \ll 2e^2/C$ the rms noise voltage vanishes in the limit that $\sigma \rightarrow 0$, because the state vector is collapsing to the definite-number state $|0\rangle$.

Figure 19 depicts the scaling characteristics of the rms noise voltage at zero temperature for the specific cases (1) $S_C = 0.64 \times 10^{-2} \mu\text{m}^2$, (2) $S_C = 0.9 \times 10^{-2} \mu\text{m}^2$, and (3) $S_C = 1.27 \times 10^{-2} \mu\text{m}^2$. The values of S_C correspond to a junction with $l/\epsilon = 1$ and (1) $j = 4.4$, (2) $j = 2.2$, and (3) $j = 1.1$. An examination of this figure reveals the following.

(1) The rms noise voltage is a maximum for $S \sim S_C$. As $S \rightarrow 0$, $\langle \delta V^2 \rangle^{1/2} \rightarrow 0$ almost linearly with junction area in accord with Eq. (5.33). Furthermore, for $S > S_C$, the rms noise voltage decreases with S in accord with Eq. (5.37).

(2) As j increases so does the rms noise voltage in accord with the discussion above. For example, in the plasmon regime $\langle \delta V^2 \rangle^{1/2}$ scales with the current density as $j^{0.15}$, whereas in the strong-

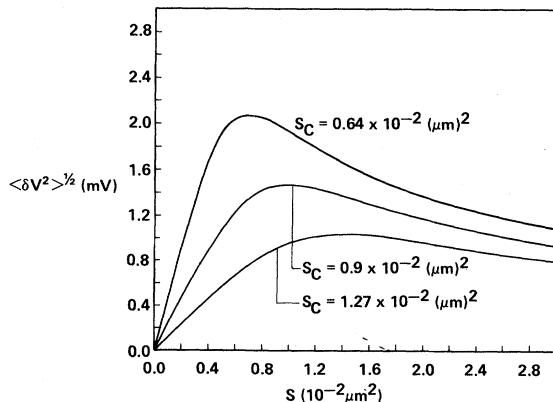


FIG. 19. Scaling characteristics of the rms noise voltage at zero temperature for (1) $S_C = 0.64 \times 10^{-2} \mu\text{m}^2$, (2) $S_C = 0.9 \times 10^{-2} \mu\text{m}^2$, and (3) $S_C = 1.27 \times 10^{-2} \mu\text{m}^2$.

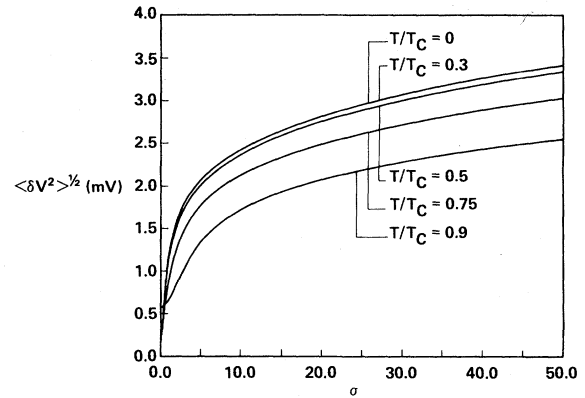


FIG. 20. Dependence of the rms voltage on σ for (1) $T/T_C = 0$, (2) $T/T_C = 0.3$, (3) $T/T_C = 0.5$, (4) $T/T_C = 0.75$, and (5) $T/T_C = 0.9$ with $T_C = 10$ K and $C = 10^{-16}$ F. The excited states are not thermally activated in this case.

charge-fluctuation regime it depends linearly on j .

(3) Note that relatively large size of the noise voltage when $S \sim S_C$. For $j = 4.4$, $\langle \delta V^2 \rangle^{1/2} \sim 2.2$ mV; if $j = 2.2$, $\langle \delta V^2 \rangle^{1/2} \sim 1.4$ mV, and if $j = 1.1$, $\langle \delta V^2 \rangle^{1/2} \sim 1.0$ mV. In contrast, we note that according to the law of corresponding states, a Josephson junction with a transition temperature of 10 K has a gap voltage of 3.1 mV.

Figures 20 and 21 depict the dependence of the rms noise voltage on the electrostatic parameter σ with the junction is biased at maximum current at the following temperatures: (1) $T/T_C = 0$, (2) $T/T_C = 0.3$, (3) $T/T_C = 0.5$, (4) $T/T_C = 0.75$, and (5) $T/T_C = 0.9$. In both figures $T_C = 10$ K, however, $C = 10^{-16}$ F in Fig. 20 and $C = 10^{-15}$ F in Fig. 21.

An examination of Fig. 20 reveals that for $\sigma \gg 1$, the rms noise voltage increases with increasing σ in accord with Eq. (5.33). Note too, that $\langle \delta V^2 \rangle^{1/2}$ de-

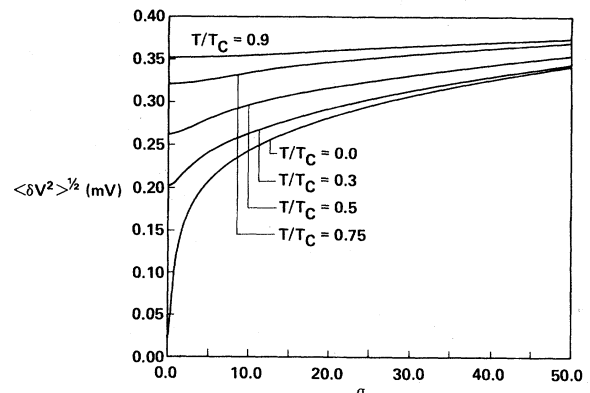


FIG. 21. Same as Fig. 20 except $C = 10^{-15}$ F and the excited states are thermally activated.

increases with increasing temperature in the plasmon regime. This feature of the junction's dynamics arises from the fact that for $C = 10^{-16}$ F and $\sigma > 10$, the plasma frequency exceeds kT_C/h , and the device is in the ground state. As noted in the discussion below Eq. (5.38), the rms noise voltage scales with temperature as $f^{0.2}(T)$ and therefore should decrease with increasing temperature. As the electrostatic parameter decreases below five, the noise voltage also decreases rapidly approaching a limiting value of E/e at low temperatures. If the capacitance is fixed, Eq. (5.39) can be written as

$$\langle \delta V^2 \rangle^{1/2} = \frac{2e}{C} \sigma \quad (5.41)$$

so that $\langle \delta V^2 \rangle^{1/2}$ decreases linearly with σ . Note that for very small values of the electrostatic parameter, the rms noise voltage does not vanish. This is due to the fact that as $T/T_C \rightarrow 1$, the excited junction states are partially activated, and the rms noise voltage is described by Eq. (5.37). Also for these cases, the higher the temperature, the larger is the limiting value of $\langle \delta V^2 \rangle^{1/2}$.

An examination of Fig. 21 reveals that the rms noise voltage increases with temperature. This arises because for $C = 10^{-15}$ F, the excited states are thermally activated and in the plasmon regime the situation is described by Eq. (5.34). Furthermore, the rms noise voltage is independent of σ in the plasmon regime, and as the device enters the strong-charge-fluctuation regime the detailed dependence on the electrostatic parameter is very sensitive to junction temperature. For example, at $T=0$, the junction is in the ground state and the noise voltage is described by Eq. (5.41). At finite temperature, the noise voltage has major contributions from the excited states, i.e., Eq. (5.35) and the terms are independent of σ .

Figure 22 depicts the temperature dependence of the rms noise voltage for a junction with $j=8.8$, $T_C=10$ K, and (1) $\sigma=500$, (2) $\sigma=50$, (3) $\sigma=5$, and (4) $\sigma=\frac{1}{2}$. Note the complex thermal behavior exhibited by $\langle \delta V^2 \rangle^{1/2}$ in the form of curve crossing as well as sudden dips near T_C .

D. Power spectrum of voltage fluctuations

The power spectrum of voltage fluctuations $P_V(\omega)$ is defined by

$$P_V(\omega) = \int_0^\infty d\tau \cos \omega \tau (\langle \hat{V}(\tau) \hat{V}(0) \rangle - \langle \hat{V} \rangle^2). \quad (5.42)$$

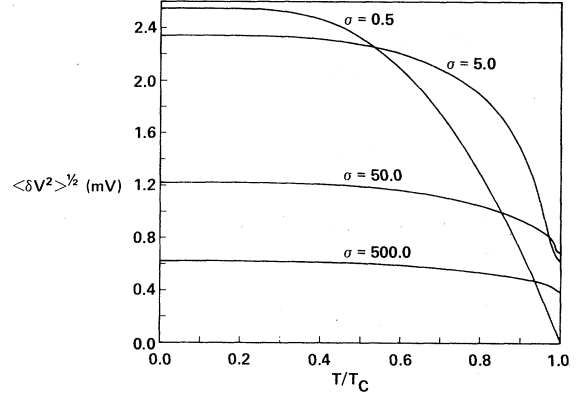


FIG. 22. Temperature dependence of the rms noise voltage for (1) $\sigma=500$, (2) $\sigma=50$, and (4) $\sigma=\frac{1}{2}$ for a junction with $T_C=10$ K and $j=8.8$.

With $\langle \hat{V} \rangle = 0$ and the insertion of a complete set of intermediate states into the voltage correlation function, Eq. (5.42) becomes

$$P_V(\omega) = \sum_{l,l'} P_l(T) |\langle \psi_l | V | \psi_{l'} \rangle|^2 \delta(\omega - \Omega_{ll'}), \quad (5.43)$$

where $\hbar\Omega_{ll'} = \epsilon_l - \epsilon_{l'}$. Once again we take finite-lifetime effects into account by introducing a phenomenological line-shape factor $g_{ll'}(\omega)$ defined by

$$g_{ll'}(\omega) = \frac{(\Gamma_l + \Gamma_{l'})/2\pi}{(\omega - \Omega_{ll'})^2 [(\Gamma_l + \Gamma_{l'})/2]^2}, \quad (5.44)$$

and the power spectrum for voltage fluctuations is

$$P_V(\omega) = \sum_{l,l'} \frac{e^{-\epsilon_l/kT}}{Z} |\langle \psi_l | \hat{V} | \psi_{l'} \rangle|^2 g_{ll'}(\omega). \quad (5.45)$$

The matrix elements $\langle \psi_l | \hat{V} | \psi_{l'} \rangle$ can be written as

$$\langle \psi_l | \hat{V} | \psi_{l'} \rangle = \frac{2e}{C} \sum_n n b_n^l b_n^{l'}. \quad (5.46)$$

1. Tight-binding limit: No electrostatic effects

In the limit that $C \rightarrow \infty$,

$$P_V(\omega) \rightarrow 0. \quad (5.47)$$

2. Plasma oscillations: Intermediate electrostatic effects

If we assume that the Γ_l are independent of l , then

$$P_V(\omega) = \langle \delta V^2 \rangle \frac{\Gamma/\pi}{(\omega - \omega_p)^2 + \Gamma^2}, \quad (5.48)$$

as all the Ω_{ll} ; that contribute to the voltage fluctuation spectrum are equal to ω_p in the limit that the plasma mode can be treated as a harmonic oscillator.

In the limit that $\hbar\omega_p \gg kT$, Eq. (5.48) is

$$P_V(\omega) = \left[\frac{\hbar\omega_p}{2C} \right] \frac{Q/\pi}{(\omega - \omega_p)^2 + \Gamma^2}. \quad (5.49)$$

Near the line center, where $\omega - \tilde{\omega}_p \ll \Gamma$, Eq. (5.49) reduces to

$$P_V(\omega) \rightarrow \frac{\hbar Q}{\pi C}, \quad (5.50)$$

which is independent of the electrostatic parameter, scales as S^{-1} with junction area, and depends on temperature only via the cavity Q . Far from the line center, where $\omega \gg \omega_p$, the voltage fluctuation spectrum reduces to

$$P_V(\omega) = \left[\frac{e}{c} \right]^3 \frac{2e}{\omega^2 Q} \sigma \cos \phi. \quad (5.51)$$

If the junction is biased at maximum current

$$P_V(\omega) = \left[\frac{e}{C} \right]^3 \frac{2e}{\omega^2 Q} \sigma^{0.8}. \quad (5.52)$$

An examination of Eq. (5.52) reveals that far from the line center, the spectrum of voltage fluctuations scales with the electrostatic parameter as $\sigma^{0.8}$, and with junction area as $S^{-1.4}$ and decreases with temperature as $f^{0.8}(T)Q(0)/Q(T)$.

If $\hbar\omega_p \ll kT$, the spectrum of voltage fluctuations is given by

$$P_V(\omega) = \left[\frac{kT}{C} \right] \frac{\Gamma/\pi}{(\omega - \omega_p)^2 + Q^2}. \quad (5.53)$$

Near the line center

$$P_V(\omega) \rightarrow kT \left[\frac{\hbar Q}{\sqrt{2}\pi e^2} \right] (\sigma \cos \phi)^{-1/2}. \quad (5.54)$$

If the junction is biased at maximum current

$$P_V(\omega) \rightarrow \frac{1}{2} kT \left[\frac{\hbar Q}{\pi e^2} \right] \sigma^{-0.4}, \quad (5.55)$$

which scales with the electrostatic parameter as $\sigma^{-0.4}$ with junction area as $(S_C/S)^{0.8}$ and increases with temperature as $Tf^{-0.4}(T)$. Far from the line center, Eq. (5.53) reduces to

$$P(\omega) \rightarrow \frac{\sqrt{2}}{\pi\omega^2} \frac{kT}{Q} \sqrt{\sigma \cos \phi}. \quad (5.56)$$

If the junction is biased at maximum current, then in the far wings

$$P_V(\omega) \rightarrow \left[\frac{kT}{\pi Q} \right] \left[\frac{e}{\omega C} \right]^2 \sigma^{0.4}, \quad (5.57)$$

which scales with the electrostatic parameters as $\sigma^{0.4}$, with the junction area as $S^{-1.2}$, and with temperature as $Tf^{0.4}(T)Q(0)/Q(T)$.

3. Strong charge fluctuations: Quenching of phase order

In the strong-charge-fluctuation regime we require matrix elements of the voltage between states of different symmetry, i.e., $\langle \psi_n^+ | \hat{V} | \psi_n^- \rangle$. To zero order in $\sigma \ll 1$, only terms diagonal in n contribute:

$$\langle \psi_n^+ | V | \psi_n^- \rangle = \frac{2en}{C}. \quad (5.58)$$

If $kT \ll 2e^2/C$ the junction is in the ground state and we require the matrix element connecting the ground state to the state $|\psi_1(\phi)\rangle$:

$$\langle \psi_0 | \hat{V} | \psi_1^- \rangle = \frac{1}{\sqrt{2}} \frac{2e}{C} \sigma \cos \phi. \quad (5.59)$$

In this limit the spectrum of voltage fluctuations is, at maximum current,

$$P_V(\omega) = \left[\frac{E}{2e} \right]^2 \frac{\Gamma/\pi}{(\omega - \Omega)^2 + \Gamma^2}, \quad (5.60)$$

where $\Omega \equiv 2e^2/\hbar C$. Near the line center,

$$P_V(\omega) \rightarrow \pi Q \sigma^2, \quad (5.61)$$

which decreases rapidly as $\sigma \rightarrow 0$. Note that at these frequencies, the spectrum of voltage fluctuations scales as $(S/S_C)^4$.

VI. DISCUSSION

In this paper, we discussed the influence of electrostatic effects on the static tunneling characteristics of single ultrasmall Josephson junctions that are current biased on the zero-voltage dc step. We found that electrostatic effects alter the phase-

dependence, magnitude as well as the scaling and thermal characteristics of the dc supercurrent from the standard expression

$$I = J \sin \phi, \quad (6.1)$$

which is valid in the tight-binding limit $C \rightarrow \infty$. Furthermore, electrostatic effects also modify the response of the pair current to applied magnetic fields and give rise to current and voltage fluctuations that accompany the flow of the supercurrent. The extent of these effects depends critically on the value of the electrostatic parameter, which in turn implies a striking sensitivity to junction dimensions for this class of devices. More precisely, since $\sigma = (S/S_C)^2$, we have for a Josephson junction whose oxide interface has dimensions $L \times L$

$$\sigma = (L/L_C)^4, \quad (6.2a)$$

$$L_C \equiv S_C^{1/2} = 0.115 \left[\frac{t}{\epsilon j} \right]^{1/4}, \quad (6.2b)$$

with L_C expressed in μm . Thus, small changes in L can give rise to sizable changes in σ which, as discussed in this study, can profoundly alter the junction's tunneling characteristics. As a specific example, we consider a junction with a current density of $1.1 \times 10^8 \text{ A/m}^2$, an oxide thickness of 30 \AA , and a dielectric constant of 3. The critical surface area $S_C = 1.27 \times 10^{-2} \mu\text{m}^2$ and if the junction's dimensions are $1.13 \times 1.13 \mu\text{m}^2$, then the electrostatic parameter is equal to 10 000. The tunneling characteristics of this device are, at maximum current,

$$\begin{aligned} J &= 1.4 \times 10^{-4} \text{ \AA}, \\ C &= 1.12 \times 10^{-14} \text{ F}, \\ I &= 1.38 \times 10^{-4} \text{ A}, \\ S/N &= 79.62, \\ \langle \delta I^2 \rangle^{1/2} &= 1.76 \mu\text{A}, \\ \langle \delta V^2 \rangle^{1/2} &= 90 \mu\text{V}. \end{aligned} \quad (6.3)$$

Thus, electrostatic effects reduce the supercurrent by about 1.5% from its tight-binding limit, give rise to a noise current of $1.76 \mu\text{A}$, and generate a noise voltage of $90 \mu\text{V}$. Suppose now we consider the effects of scaling down the junction's linear dimensions by a factor of 10, i.e., $L = 0.113 \mu\text{m}$ and $\sigma = 1$. For this device, we have, at zero temperature,

$$\begin{aligned} J &= 1.4 \mu\text{A}, \\ C &= 1.12 \times 10^{-16} \text{ F}, \\ I &= 0.49 \mu\text{A}, \\ S/N &= 0.55, \\ \langle \delta I^2 \rangle^{1/2} &= 0.89 \mu\text{A}, \\ \langle \delta V^2 \rangle^{1/2} &= 1.05 \text{ mV}. \end{aligned} \quad (6.4)$$

Thus, for this case, electrostatic effects have reduced the supercurrent to about $\frac{1}{3}$ of its tight-binding value. Hence, scaling the junction down by a factor of 100 has reduced the supercurrent by a factor 286. Furthermore, despite the difference in junction size, the noise current has been reduced only by a factor of 2 and the signal-to-noise ratio has decreased to about $\frac{1}{2}$. In addition, the rms noise voltage has increased by more than 1 order of magnitude to 1.05 mV , which is equal to the gap voltage of In and is about $\frac{1}{3}$ the gap voltage of Pb. Finite temperatures will further decrease the size of the supercurrent as well as the signal-to-noise ratio. Thus, scaling down the junction's dimensions from the $1\text{-}\mu\text{m}$ regime to $0.1\text{-}\mu\text{m}$ regime will extensively alter its tunneling characteristics. Below, we summarize our findings and discuss some of the technological implications of this research.

If $S \gg S_C$, the junction is in the plasmon regime which in general involves devices whose linear dimensions are on the order of $1 \mu\text{m}$ or more. For example, if the junction is operated at low temperatures such that $kT \ll \hbar\omega_p$ and biased at maximum dc current, electrostatic effects will induce phase fluctuations

$$\langle \delta \theta^2 \rangle = (S_C/S)^{0.8}, \quad (6.5)$$

which will increase as the device is scaled down in size. Furthermore, these phase fluctuations will reduce the supercurrent so that its maximum value is no longer J but

$$I = J \left[1 - \frac{5}{8} \left(\frac{S_C}{S} \right)^{0.8} \right], \quad (6.6)$$

so that for $S = 10S_C$, electrostatic effects will reduce the supercurrent by about 10%. Furthermore, electrostatic fluctuations will alter the magnetic and thermal characteristics of the junction from the ideal tight-binding limit. For example, the pair-current's response to dc magnetic fields will be most noticeably altered in the vicinity of the zeros in the diffraction pattern. Thus, for a range of field strength's δH about the diffraction zero,

$$\delta H = 4\pi n H_n \left[\frac{S_C}{S} \right]^{1.6}, \quad (6.7)$$

the diffraction pattern will be significantly altered from $(\text{sink}L)/kL$. In Eq. (6.7), n is the order of the diffraction zero and H_n the associated field strength. Thus, for a $1\text{-}\mu\text{m}$ device with $S=10S_C$, $\delta H \sim 0.315H_1$, where H_1 is typically 500 G. In addition, as $T/T_C \rightarrow 1$, the pair current varies with temperature as

$$I(T) = I(0)[1 - T/T_C] \times \left[1 - \frac{5/8}{(1 - T/T_C)^{0.4}} \left[\frac{S_C}{S} \right]^{1/6} \right], \quad (6.8)$$

provided the excited states are not thermally activated. If $kT \gg \hbar\omega_p$, the supercurrent is further suppressed,

$$I(T) = J(T) \left[1 - \frac{3}{2} \left[\frac{kT}{E(T)} \right]^{1/3} \right], \quad (6.9)$$

and the tunneling characteristics are appropriately altered.

Associated with the flow of a supercurrent are current and voltage fluctuations, which are given by

$$\langle \delta I^2 \rangle^{1/2} = \frac{1}{2} J \left[\frac{S_C}{S} \right]^{0.8}, \quad (6.10a)$$

$$\langle \delta V^2 \rangle^{1/2} = \frac{e}{C} \left[\frac{S}{S_C} \right]^{0.4}, \quad (6.10b)$$

provided the excited states are not thermally activated and the junction is biased at maximum current. Note that the noise current is almost independent of area, in this regime, but the signal-to-noise ratio

$$\frac{S}{N} = 2 \left[\frac{S}{S_C} \right]^{0.8}, \quad (6.11)$$

decreases rapidly if the device is scaled down in size. Furthermore, the noise voltage also increases as the junction area decreases, scaling as $S^{-0.6}$. If the excited states are thermally activated, the noise current and voltage scale as

$$\langle \delta I^2 \rangle^{1/2} = J \left[\frac{kT}{E} \right]^{5/6},$$

$$\langle \delta V^2 \rangle^{1/2} = \left[\frac{kT}{C} \right]^{1/2}.$$

In general, further reduction in device size gives rise to smaller pair currents, decreasing signal-to-noise ratios, slightly smaller noise currents, and large noise voltages, provided the junction remains in the plasmon regime. For the ground state, this requires $S \geq 6S_C$. However, electrostatic fluctuations are greater in the excited states which as S decreases first become anharmonic and then exhibit positive energy eigenvalues.

If the junction is further scaled down in size, the excited states can no longer be regarded as plasma oscillations. For device areas on the order of several times the critical surface area, these states become either pairwise degenerate or quasidegenerate. In addition, the direction of current flow of the higher excited states is opposite to that of the ground and first excited state as S decreases below $5S_C$, i.e., $A_3 < 0$ for $S/S_C < 4.73$ and $A_2 < 0$ for $S/S_C < 3.67$ when the device is biased at maximum current. Furthermore, as the junction area is reduced from $3S_C$ down to S_C , electrostatic effects reduce the supercurrent from about $\frac{4}{5}J$ to $\frac{1}{3}J$. Within this regime (where σ drops from 9 to 1) the scaling, magnetic, and thermal characteristics of the Josephson current undergo qualitative changes in its functional dependence on junction area, magnetic flux penetration, and temperature. At zero temperature, the signal-to-noise ratio falls from about 2.6 down to about 0.6, implying that the noise current varies almost linearly with junction area. The noise voltage continues to increase reaching a maximum at $S=S_C$. For example, if $S_C = 0.64 \times 10^{-2} \mu\text{m}^2$, the noise voltage increases from approximately 1.4 to 2.2 mV. Furthermore, the smaller the value of S_C , the larger is $\langle \delta V^2 \rangle^{1/2}$, e.g., if $S_C = 0.45 \times 10^{-2} \mu\text{m}^2$, $\langle \delta V^2 \rangle^{1/2} = 2.9$ mV when $S=S_C$. Typical device sizes in this regime are on the order of $0.1 - 0.2 \mu\text{m}$.

As the junction size is scaled down even further, so that $S < S_C$, the device enters the strong-charge-fluctuation regime where electrostatic effects quench the phase ordered state and the tunneling interaction can be regarded as a weak perturbation. In this regime, the eigenvectors and eigenvalues rapidly approach the electrostatic values

$$|\psi_n^\pm(\phi)\rangle \rightarrow \frac{1}{\sqrt{2}} (e^{-in\phi} |n\rangle \pm e^{in\phi} |-n\rangle), \quad (6.12a)$$

$$\epsilon_n^\pm \rightarrow \frac{(2en)^2}{2C}, \quad (6.12b)$$

with corrections of order $(S/S_C)^2 \ll 1$, arising from pair transfer. These perturbations tend to broaden

the distribution in n space, so that in the ground state

$$\langle \delta \hat{n}^2 \rangle = \left[\frac{S}{\sqrt{2}S_C} \right]^4, \quad (6.13)$$

which is much less than unity. For example, if $S/S_C=0.25$, the rms number fluctuations is of the order of 0.03, which implies that the pair phase is completely undefined in this regime. Despite this fact, pair transfer is still possible; however, before summarizing the tunneling characteristics of this regime, we first estimate typical device dimensions. For a junction with a critical current density of 1.1×10^8 A/m², an oxide thickness of 30 Å, and a dielectric constant of 3, $S_C=1.27 \times 10^{-2}$ μm² and $L_C=0.11$ μm. It follows that typical linear dimensions in this regime are 0.08 μm, so that $S=0.64 \times 10^{-2}$ μm² and $\sigma=0.28$.

In the strong-charge-fluctuation regime, electrostatic effects dominate the junction's dynamics and profoundly alter the phase dependence of the pair current as well as its scaling, magnetic, and thermal characteristics. In particular, if $kT \ll 2e^2/C$ so that the junction is in the ground state,

$$I = \frac{1}{2} J_C \left[\frac{S}{S_C} \right]^3 \sin 2\phi, \quad (6.14)$$

which implies an extreme sensitivity to the device's linear dimensions. Specifically, if $S/S_C \lesssim 0.25$, electrostatic effects will reduce the supercurrent to about $0.03J$. Thus if $S_C=0.01$ μm² and the critical current density is 1.76×10^8 A/m², then the maximum supercurrent will be on the order of 13 nA. Electrostatic effects alter the supercurrent's response to magnetic field, so that

$$I(H) = I(0) \left[\frac{\sin kL}{kL} \right]^2. \quad (6.15)$$

Note, that the first zero in the diffraction pattern occurs at field strengths on the order of 5000 G or more. Equation (6.15) also implies altered superconducting quantum-interference device (SQUID) characteristics due to the current-phase relationship. For a SQUID consisting of two identical ultrasmall Josephson junctions in the strong-charge-fluctuation regime, the maximum current in the loop is

$$I = J \left[\frac{S}{S_C} \right]^2 \cos \left[\frac{2e}{h} \Phi \right]. \quad (6.16)$$

In Eq. (6.17) Φ is the magnetic flux penetrating the loop, and we have neglected the effects of flux

penetrating the junctions themselves (which is of order L/R , where R is the radius of the loop). Thus, the flux periodicity of this modulation is of order $h/4e$ instead of $h/2e$. We plan to discuss the SQUID characteristics of ultrasmall Josephson junctions elsewhere.

The magnitude of the junction current is also quite sensitive to the temperature, even if the device is operating in the ground state, since

$$I(T) = I(0) \left[\frac{\Delta(T)}{\Delta(0)} \tanh \frac{\Delta(T)}{2kT} \right]^2. \quad (6.17)$$

Thus, the supercurrent will be independent of temperature over a much narrower range than larger junctions. For example, in standard devices the current will vary with temperature by only 10% in the range $0 \leq T/T_C \leq \frac{1}{2}$. According to Eq. (6.17) the range is narrowed to $0 \leq T/T_C \leq \frac{1}{4}$, provided the excited junction states are not thermally activated. If they are, then this range will be further narrowed.

Accompanying the supercurrent is a noise current that arises from order-disorder fluctuations, which is given by

$$\langle \delta I^2 \rangle^{1/2} = \frac{I}{\sqrt{2}} J, \quad (6.18)$$

and for the junction parameters quoted just below Eq. (6.13) is about 0.5 μA at zero temperature. In this regime, the signal-to-noise ratio is of order $(S/S_C)^2 \ll 1$. However, observation of pair currents in this regime may still be possible due to the fact that the spectrum of current fluctuations is peaked at the electrostatic frequency $\Omega = 2e^2/\hbar C$, which is typically on the order of 10^{12} Hz. If a narrow bandwidth detector is used, only a small fraction of the current fluctuations will contribute to the rms noise current, and the signal-to-noise ratio will exceed unity. Note that since the current varies as $J^2 C$, detection of such currents is most favored by using junctions with values of J as large as possible, which are consistent with the requirement that $\sigma \ll 1$.

In the strong-charge-fluctuation regime, the rms noise voltage is given by

$$\langle \delta V^2 \rangle^{1/2} = \frac{\hbar J}{2e^2}, \quad (6.19)$$

provided that the excited junction states are not thermally activated. For this situation, the noise voltage scales linearly with area and therefore decreases as the device dimensions are scaled down. Typical noise voltages in this regime for junctions

with critical current densities of 1.1×10^8 A/m² and areas of 10^{-14} m² are 2 mV, which is less than the gap voltage of a Pb-PbO-Pb junction.

In addition to the tunneling characteristics of the supercurrent, we have also examined a model of the external circuit that we believe is suitable for ultrasmall Josephson junctions. We note that our model reduces to Anderson's model of the external circuit for large junctions but does not suffer from its difficulties when applied to ultrasmall devices. We believe that this model, if used in conjunction with the theory presented in this paper, should be suitable for examining fluctuation induced switching in ultrasmall Josephson junctions.

Next, we comment on some of the technological implications of this research with regard to digital applications of ultrasmall Josephson junctions. In particular, we briefly discuss: (1) size tolerances for device fabrication, (2) thermal ranges concerning junction operation, (3) aspects of switching schemes, and (4) voltage fluctuations. We stress that these observations are preliminary in nature and based solely on this study. Other aspects concerning the operational characteristic of ultrasmall Josephson junctions must first be examined before all of the issues are clear.

We begin by noting that once $S \lesssim 3S_C$, the supercurrent exhibits a very sensitive dependence on the device dimensions. Accordingly, size tolerance in the fabrication of ultrasmall Josephson junctions is extremely important if one is to ensure uniform switching characteristics of these devices on a chip. This statement is underscored by noting that a 20% variation in junction area about $S = 2S_C$ will give rise to a factor-of-2 variation in the maximum zero-voltage dc supercurrent. In the strong-charge-fluctuation regime, this trend becomes extreme. For example, a 25% variation in device area about $S = 0.5S_C$ gives rise to almost a factor-of-5 variation in the maximum zero-voltage pair current. Thus, if $S_C = 0.64 \times 10^{-2}$ μm² (at zero temperature) and S varies from 0.24×10^{-2} to 0.4×10^{-2} μm², the size of the current will change from $0.026J_C$ to $0.12J_C$ and the signal-to-noise ratio will vary from 0.05 to 0.3, i.e., a factor-of-6 variation. On the other hand, within this same range, the noise voltage will vary from 1.1 mV (for the smaller device) to 1.7 mV.

Reliable operation of ultrasmall Josephson junctions will involve reduced thermal tolerances, as the device will have to be operated within a narrower temperature range if undesirable switching is to be avoided. For example, between $T/T_C = 0.0$ and 0.75, the maximum dc pair current for a larger de-

vice (i.e., $S > 10$ μm²) will vary by about 27%. For an ultrasmall device, with $S \sim 3S_C$, the magnitude of the pair current will vary by a factor of 3, provided the excited states are not thermally activated. If they are thermally activated, then the magnitude of the supercurrent will virtually vanish. To ensure that the supercurrent will remain nearly constant over a given temperature range, the results of this study indicate that the device's operational temperature should satisfy

$$(1) \quad 0 \leq T \leq \frac{1}{4}T_C,$$

$$(2) \quad kT \ll 2e^2/C.$$

In contrast, larger junctions require $0 \leq T \leq \frac{1}{2}T_C$, and there is no analog of (2). We note that fluctuation induced switching may impose additional constraints as well as narrower tolerances than those mentioned above.

Another feature of ultrasmall Josephson junctions is that only a small amount of flux can penetrate the device (i.e., kL is small due to $L \sim 0.1$ μm or so), and very large magnetic fields would, in general, be required to switch a single device. Thus, logic based on single junctions would be much more feasible if current switching is employed. Note, however, that this is not necessarily the case if SQUID's are used as the basic switching element.

One can, of course, attempt to reduce the scaling difficulties noted above by using junctions with larger critical current densities. Since the critical junction size scales of $j^{-1/2}$, it follows that by increasing j by 1 order of magnitude, S_C will decrease by a factor of more than 3. Thus a device with a critical current density of 8.8×10^8 A/m², an oxide thickness of 25 Å, and a dielectric constant of 2.2 has $S_C = 0.36 \times 10^{-2}$ μm² and the critical linear dimension is $L_C \simeq 0.6$ μm instead of 0.1 μm as stated above. There are, however, limitations to this. Larger current densities will probably impose stricter quality control on both materials as well as junction fabrication. In addition, current densities exceeding 10^{10} A/m² are probably unlikely. A more promising approach is to use devices whose oxides have larger dielectric constants. For example, ZnO has a static dielectric constant of 4.6, PbO one of 8.4, and for Nb oxide it is even higher. However, during switching processes, the dynamic properties of the oxide's dielectric function will be important, and these functions typically peak in the vicinity of $10^{12} - 10^{13}$ Hz, which also coincides with the gap voltage. Since the larger the static dielectric constant, the greater will be this variation, it is unclear that using materials whose oxide dielectric constants are large is a viable solution. Note too that

the larger the dielectric constant, the slower the switching time.

Voltage fluctuations are also a very important feature in considering the digital applications of Josephson junctions. In general, one requires

$$\langle \delta V^2 \rangle^{1/2} \ll V_g = 2e\Delta, \quad (6.20)$$

i.e., the rms noise voltage must be much less than the gap voltage if one is to avoid undesirable switching events. One result of this study is that the noise voltage peaks at $S \sim S_C$. Furthermore, it increases with increasing current, achieving maximum values of $\langle \delta V^2 \rangle^{1/2} = 2.9$ mV for $S_C = 0.45 \times 10^{-2} \mu\text{m}^2$, $\langle \delta V^2 \rangle^{1/2} = 2.2$ mV for $S_C = 0.64 \times 10^{-2} \mu\text{m}^2$, $\langle \delta V^2 \rangle^{1/2} = 1.4$ mV for $S_C = 0.9 \times 10^{-2} \mu\text{m}^2$, and $\langle \delta V^2 \rangle^{1/2} = 1.0$ mV for $S_C = 1.27 \times 10^{-2} \mu\text{m}^2$. It is also worth recalling that the rms noise voltage scales with junction area as $S^{-0.6}$ (if the device is in the ground state) and $S^{-0.5}$ (if the excited states are thermally activated)

so that the noise voltage remains relatively large even for $S \sim 5 - 10S_C$. On the other hand, the noise voltage decreased almost linearly with junction area for $S < S_C$. For example, for $S = \frac{1}{2}S_C$, $\langle \delta V^2 \rangle^{1/2} \sim 1.4$ mV for the case $S_C = 0.45 \times 10^{-2} \mu\text{m}^2$. Thus small size does have some operational advantages.

We have not considered the effects of fluctuations switching the junction out of the zero-voltage state. For larger junctions, this effect is manifested through a slanting $I(V)$ characteristics and results in a reduced maximum critical current.^{15,16} Theories treating fluctuation-induced switching are based on the notion of a well-defined phase. As previously noted, we are considering a junction in which the phase cannot be regarded as a well-defined classical variable as the two superconducting electrodes are only partially correlated. We plan to examine fluctuation-induced switching effects for ultrasmall junctions elsewhere.

¹IBM J. Res. **24**, (2) (1980).

²J. Matisoo, Sci. Am. **242**, 50 (1980).

³D. Rogovin, Phys. Rev. Lett. **45**, 836 (1980); also D. Rogovin and J. Nagel, *ibid.* **46**, 1238 (1981).

⁴D. Rogovin, J. Nagel, and M. Scully, Phys. Rev. B **23**, 1156 (1981).

⁵P. W. Anderson, in *Lectures on the Many-Body Problem*, edited by E. Cainaniello, (Academic, New York, 1964).

⁶J. R. Schrieffer, *Superconductivity* (Benjamin, New York, 1964).

⁷M. Abramowitz and G. Stegun, *Handbook of Mathematical Functions* (Dover, New York, 1980).

⁸R. Ferrell and R. Prange, Phys. Rev. Lett. **10**, 479 (1963).

⁹P. W. Anderson, in *Progress in Low Temperature Physics*, edited by C. J. Gorter (North-Holland, Amsterdam, 1967), Vol. V.

¹⁰The authors are indebted to M. Scully and S. Stenholm for this proof.

¹¹M. Silverman, Phys. Rev. A **24**, 339 (1981).

¹²A discussion of some of the effects of plasma oscillations on the supercurrent is given by D. J. Scalapino, in *Tunneling Phenomena in Solids*, edited by S. Lundquist and E. Burnstein (Dekker, New York, 1969).

¹³Some of the material presented here is discussed by D. Rogovin and J. Nagel, App. Phys. Lett. **39**, 994 (1981).

¹⁴In addition to fluctuations in the pair current, there are also quasiparticle current fluctuations which have been discussed extensively by D. Rogovin and D. J. Scalapino, [Ann. Phys. (N.Y.) **84**, 1 (1974)] and are not considered.

¹⁵Y. Ivanchenko and L. Zillberman, Zh. Eksp. Teor. Fiz. **55**, 2395 (1968) [Sov. Phys.—JETP **28**, 1272 (1969)]; **58**, 211 (1970) [**31**, 117 (1970)]. Other aspects of this problem for large devices have been examined by V. Ambegaokar and B. J. Halperin, Phys. Rev. Lett. **22**, 1364 (1969).

¹⁶R. Voss and R. Webb, Phys. Rev. Lett. **47**, 265 (1981), and references therein.